J. Fluid Mech. (1987), *vol.* 174, *pp.* 155–185
Printed in Great Britain

The scattering of light by a chaotically convecting fluid

By SUSAN C. RYRIE
School of Mathematics, University of Bristol, University Walk, Bristol BS8 1TW, UK

(Received 17 July 1985 and in revised form 19 May 1986)

The way in which light, scattered by a thin layer of fluid, may be used to obtain quantitative information about the temperature field in the fluid is investigated. Expressions for the phase shift imposed by the fluid, and the intensity of the scattered light are derived in terms of the Fourier representation of the temperature field, under the assumption of small variations in the refractive index. The method is applied to the particular case of chaotic convection, with a view to studying the connection between strange attractors and turbulence. Two simple mathematical models of chaotic convection are studied; particular emphasis is attached to the statistical properties of the flow and of the scattered light field, which are calculated numerically.

1. Introduction

The study of the transition to turbulence has been given much impetus by the discovery of strange attractors. These sets may appear in the solution spaces of nonlinear dynamical systems, when the control parameters take certain values. In contrast to the 'classical' attractors (fixed points or limit cycles), strange attractors have non-integer fractal dimensions. Also, orbits upon such attractors are usually chaotic; that is, they are aperiodic and sensitive to initial conditions. Thus two orbits emanating from points arbitrarily close on such an attractor diverge and eventually follow completely separate paths. These last two properties are also characteristic of turbulent flows: the idea that turbulence might be related to strange attractors was proposed by Ruelle & Takens (1971).

Since the motion of a fluid is governed by partial differential equations, the relevance of solutions to systems of ordinary differential equations to understanding this motion may not be immediately obvious. However, on taking appropriate Galerkin expansions, the partial differential equations may be transformed into an infinite set of coupled ordinary differential equations governing the time-evolution of the expansion coefficients. Moreover, under certain conditions, the behaviour of the exact solution to this system is determined by the behaviour of a finite number of terms (Foias & Temam 1983). Conversely, it is well known that when insufficient terms are retained, the behaviour of the system may vary considerably with the order of truncation (cf. Curry *et al.* 1984). The problem of identifying appropriate truncations remains to be solved. Thus care must be taken in attempting to relate the solutions of truncated systems to real fluid flows. However, by studying relatively simple, severely truncated systems we might hope to identify qualitative features characteristic of chaotic flows which are present in higher-order, more realistic models.

Remote-sensing techniques have also contributed greatly to the study of

turbulent flows. They allow measurements to be made without disturbing the fluid – an important factor when the flow is unstable. The velocity of the fluid may be measured by laser-Doppler anemometry. However, measurements of the temperature field, using light-scattering techniques, are usually only qualitative.

The work described here concerns both the connection between strange attractors and turbulence, and how light-scattering techniques may be made more quantitative. It forms part of a project to study chaotic convection in a thin, horizontal layer of fluid heated from below, by comparing statistical properties of experimental results with those obtained from mathematical models. This paper reports on the theoretical work. A comparison of the results shown here with those of preliminary experiments carried out at RSRE, Malvern, by Dr J. Walker, is encouraging; the experimental work will be reported upon elsewhere, on completion of the programme.

Section 2 deals with the theory of light-scattering. A uniform, parallel beam of light is assumed to shine vertically through the fluid. Some simplifying approximations are made, and expressions obtained for the intensity of light beyond the fluid, and the phase difference between light leaving and entering the fluid. Although we consider only the particular geometrical configuration relevant to the problem of Bénard convection, much of the theory is applicable to any general region of fluid provided it is, in a certain sense, thin, and provided variations in the refractive index are small.

Section 3 contains a brief review of the theory of Bénard convection, and the modal expansions appropriate for the idealized configuration of an infinite layer of fluid, bounded in the vertical by free, perfectly conducting boundaries.

In §§4 and 5, two simple models, obtained from severe truncations of the modal expansions of Bénard convection, are discussed: the well-known Lorenz model, and a model with nine variables. Although neither is expected to describe accurately convection in a real fluid, through their simplicity they clearly demonstrate the processes involved in the scattering of light by a fluid. Consideration of these models enables us to assess the advantages of taking measurements of the phase of the scattered light, as opposed to those of its intensity. In addition, since both produce chaotic flows, we might hope they will show those qualitative features which are characteristic of chaos, and which might therefore also be present in more realistic models of convection in a fluid.

We concentrate on the statistical properties of the flow: probability density functions (or, more correctly, local times), correlation functions and averages. Since chaotic systems are usually found heuristically to be statistically stationary, ergodic and mixing, we use time averages rather than ensemble averages. Note, however, that ergodicity has been proved rigorously only for special types of systems (Lanford 1981).

In general, statistical properties must be calculated numerically: some analytical relationships exist between moments and correlation functions, but the systems cannot be closed to give explicit results. Since the sensitivity to initial conditions causes a numerically integrated orbit to diverge from the true orbit as truncation and discretization errors accumulate, one might question the accuracy of numerical results. However, Smith (1977) and Benettin *et al.* (1978) have found that numerical results for some systems are independent of truncation error and integration routine. Moreover, it might be argued that imperfections in the numerical integration are analogous to those occurring in real systems (e.g. external noise from weak vibrations).

2. Optical theory

Consider a beam of light travelling through a region in which there are small variations of the refractive index, $n(\boldsymbol{r})$, so that

$$n(\boldsymbol{r}) = n_0[1-\epsilon n_1(\boldsymbol{r})], \tag{2.1}$$

where $n_1(\boldsymbol{r}) = O(1)$, and $\epsilon \ll 1$. The path, $\boldsymbol{R}(s) = (x(s), y(s), z(s))$, of a ray is governed by the equation

$$\frac{\mathrm{d}}{\mathrm{d}s} n(\boldsymbol{R}) \frac{\mathrm{d}\boldsymbol{R}}{\mathrm{d}s} = \nabla n(\boldsymbol{R}) \tag{2.2}$$

(cf. Jones 1964 p. 343), where s is the distance along the ray from some reference point upon it. Appropriate boundary conditions on (2.2), which are convenient for our purposes, specify the position and direction of travel of the ray at $s = 0$. Also for convenience we choose the axes (x, y, z) such that at the point $s = 0$, the ray travels in the direction of the positive z-axis.

A useful approximation to (2.2) may be made by expanding

$$\boldsymbol{R}(s) = \boldsymbol{R}_0(s) + \epsilon \boldsymbol{R}_1(s) + \ldots, \tag{2.3}$$

and

$$n(\boldsymbol{R}) = n(\boldsymbol{R}_0) + \epsilon \boldsymbol{R}_1 \cdot \nabla n(\boldsymbol{R}_0) + \ldots, \tag{2.4}$$

as Taylor series. Then since

$$\left.\frac{\mathrm{d}\boldsymbol{R}}{\mathrm{d}s}\right|_{s=0} = (0, 0, 1), \tag{2.5}$$

it may be shown that

$$\boldsymbol{R}_0(s) = \boldsymbol{R}(0) + s\boldsymbol{k}, \tag{2.6}$$

where $\boldsymbol{k}$ is the unit vector in the direction of the positive z-axis. Thus to a first approximation the ray is undeflected. Moreover,

$$z_1(s) \equiv 0, \tag{2.7}$$

and a solution of (2.2) which is correct to order ϵ^1 may be found by replacing s by z. This is the paraxial approximation, under which the path of a ray is $\boldsymbol{R}_\mathrm{p}(z) = (x_\mathrm{p}(z), y_\mathrm{p}(z), z_0 + z)$ where

$$\frac{\mathrm{d}}{\mathrm{d}z}\left(n\frac{\mathrm{d}x_\mathrm{p}}{\mathrm{d}z}\right) = \frac{\partial n}{\partial x}, \quad \frac{\mathrm{d}}{\mathrm{d}z}\left(n\frac{\mathrm{d}y_\mathrm{p}}{\mathrm{d}z}\right) = \frac{\partial n}{\partial y}. \tag{2.8}$$

It is worth noting that equations (2.8) remain valid when the angle of incidence to the z-axis is non-zero, but $O(\epsilon)$ as $\epsilon \to 0$ as outlined in the author's thesis (Hawkins 1984). Thus there is a margin for error, albeit very small, in the alignment of the beam; this may be very important in experiments.

Since we are interested in studying Bénard convection, we consider the system relevant to this problem, as shown in figure 1. We wish to calculate the intensity of light in the region $z > 0$, and also the phase of light as it crosses the plane $z = 0$.

From the paraxial approximation, a ray entering the fluid at the point $(x_0, y_0, -1)$ follows the path $\boldsymbol{R}(z)$ where

$$\boldsymbol{R}(z) = (x_0, y_0, z-1) + O(\epsilon) \quad \text{as } \epsilon \to 0, \tag{2.9}$$

for any form of $n_1(\boldsymbol{r})$. The phase difference between any two points on a ray is proportional to the optical path length, along the ray, between these points:

$$\phi(\boldsymbol{R}(S)) = \phi(\boldsymbol{R}(0)) + k\int_0^S n(\boldsymbol{R}(s))\,\mathrm{d}s, \tag{2.10}$$

where k is the wavenumber of the light.

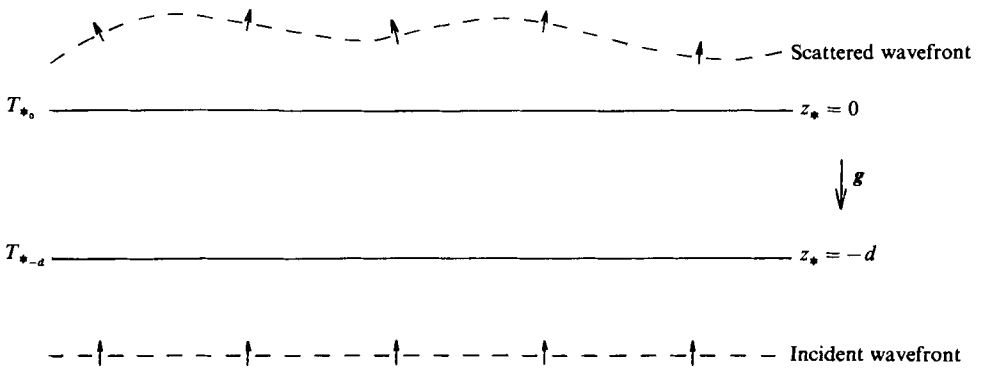

FIGURE 1. Schematic diagram of the Bénard experiment.

Therefore, on expanding the refractive index as a Taylor series about the leading-order solution (2.9), the phase of a ray entering the fluid at $(x_0, y_0, -1)$ and emerging at $(x_e, y_e, 0)$, is

$$\phi(x_e, y_e, 0) = \phi(x_0, y_0, -1) + kn_0 \int_0^{1+O(\epsilon^2)} [1 - \epsilon n_1(x_0, y_0, s) + O(\epsilon^2)]\, ds. \quad (2.11)$$

Thus the phase may be calculated correctly to order ϵ by assuming the light travels straight through the fluid without being refracted, and it is consistent with this approximation to set $(x_e, y_e) = (x_0, y_0)$. Moreover, there can be no focusing within the fluid in this approximation, and the intensity of the emerging beam is the same as that of the incident beam. This is equivalent to treating the fluid as a phase screen at the plane $z = 0$; that is, to taking its sole effect to be that of impressing the phase shift $\phi(x_0, y_0, 0) - \phi(x_0, y_0, -1)$ upon light as it crosses the plane $z = 0$.

The intensity of light observed at a point (x, y, z) is the square of the amplitude of the wave function, Ψ, there. This may be calculated from the diffraction integral, accumulating contributions from all points $(x+\xi_x, y+\xi_y, 0)$ on the phase screen. When the phase screen is paraxial, that is when

$$\frac{1}{k}\left|\frac{\partial \phi}{\partial x_0}\right| \ll 1, \quad \frac{1}{k}\left|\frac{\partial \phi}{\partial y_0}\right| \ll 1, \quad (2.12)$$

the diffraction integral may be approximated by

$$\Psi(x, y, z) \approx \frac{-ik \exp[i(kz - \omega t)]}{2\pi z} \times \int_{-\infty}^{\infty}\int_{-\infty}^{\infty} \exp\left[i\left(\phi(x+\xi_x, y+\xi_y) + k\left(\frac{\xi_x^2 + \xi_y^2}{2z}\right)\right)\right] d\xi_x\, d\xi_y \quad (2.13)$$

(Berry 1977), assuming unit intensity for the incident light. In general, it may not be possible to evaluate the integral in (2.13) exactly. However, it may be approximated in the geometrical optics limit as $k \to \infty$ by using the method of stationary phase (cf. Bleistein & Handelsman 1975). Thus

$$\Psi(x, y, z) \sim \frac{i \exp[i(kz - \omega t)]}{z|\det \Phi|^{\frac{1}{2}}} \quad \text{as } k \to \infty, \quad (2.14)$$

where

$$\Phi_{ij} = \frac{\partial^2}{\partial \xi_i \partial \xi_j}\left[\frac{1}{k}\phi(x+\xi_x, y+\xi_y) + \frac{\xi_x^2 + \xi_y^2}{2z}\right]_{(\xi_x^s, \xi_y^s)} \qquad \xi_1 = \xi_x, \quad \xi_2 = \xi_y. \quad (2.15)$$

The point (ξ_x^s, ξ_y^s) is the stationary point of the exponent, defined by

$$\mathbf{0} = \frac{\boldsymbol{\xi}^s}{z} + \frac{1}{k}\frac{\partial}{\partial \boldsymbol{\xi}}\phi(x+\xi_x, y+\xi_y)\Big|_{\xi=\xi^s}. \tag{2.16}$$

The value of the intensity follows immediately:

$$I(x,y,z) = |\Psi(x,y,z)|^2 \sim |z^2 \det \Phi|^{-1} \quad \text{as } k \to \infty. \tag{2.17}$$

Note that (2.17) is the leading-order solution for the intensity and terms of order ϵ within it must be ignored.

Equations (2.14)–(2.17) are valid provided that $\det \Phi \neq 0$: the points at which the determinant vanishes are where caustics are formed and geometrical optics breaks down. An alternative method of evaluating the intensity is to use the geometrical optics result that the intensity at a point is proportional to the density of rays there. The leading-order solution is identical to that found by the phase screen method: details are given by Hawkins (1984).

The theory described above is also valid when the refractive-index field varies slowly with time. Provided

$$\left|\frac{\partial n}{\partial t}\right| \ll \frac{c}{d} \tag{2.18}$$

(where c is the speed of light) the refractive-index field changes by a negligible amount in the time taken for the light to travel through the fluid, and may be treated as quasi-static. In this case, note that if z is so large that the inequality

$$\left|\frac{\partial n}{\partial t}\right| \ll \frac{c}{z}, \tag{2.19}$$

is violated, there is a time lag of $\tau \approx z/c$ between the phase screen and the intensity at (x,y,z).

Although we have considered a refracting region of a particular shape, it may be possible to apply the methods described above to other systems. The important requirement, besides that of small variations in the refractive index, is that to leading order there is no change of intensity within the fluid. This is true only when $x_1(z) = O(1)$ and $y_1(z) = O(1)$ at all levels z within the fluid. Now from the paraxial approximation, given that $\mathrm{d}x_1/\mathrm{d}z|_{z_0} = 0$,

$$x_1(z) = -\int_{z_0}^{z}\int_{z_0}^{\zeta} \frac{\partial n_1}{\partial x}(x_0, y_0, \chi)\,\mathrm{d}\chi\,\mathrm{d}\zeta, \tag{2.20}$$

and similarly for $y_1(z)$. Thus the phase screen approximation may not be valid when the integral in (2.20) becomes large. In particular, it may not be valid for thick layers of fluid.

3. The convection problem

We consider convection of a Boussinesq fluid confined to the region $-d \leqslant z_* \leqslant 0$, $-\infty < x_*, y_* < \infty$ (cf. Drazin & Reid 1982), where the asterisk subscript denotes a dimensional quantity and where the positive z-axis is taken vertically upwards. We denote the kinematic viscosity of the fluid by ν, the thermal conductivity by κ, the coefficient of cubical expansion by α, and the density by ρ, and take the unit of length to be d, that of time d^2/κ, of velocity κ/d, of temperature $\kappa\nu/\alpha g d^3$ and of pressure $\rho_{-d}\kappa^2/d^2$ where ρ_{-d} is the density at a reference temperature T_{-d}.

In dimensionless form the velocity, temperature and pressure fields in the steady state are

$$\boldsymbol{U} = \mathbf{0}, \quad T = T_{-d} - (T_{-d} - T_0)(z+1), \tag{3.1a, b}$$

and

$$P = P_{-d} - \frac{[\frac{1}{2}\alpha\rho d(z+1)^2 + (z+1)]gd^3}{\kappa^2}, \tag{3.1c}$$

where T_{-d} and T_0 are the temperatures of the lower and upper boundaries respectively. The perturbations $\boldsymbol{u} = (u, v, w)$, θ and p about the steady state satisfy the equations

$$\boldsymbol{\nabla}\cdot\mathbf{u} = 0, \quad \frac{\partial \boldsymbol{u}}{\partial t} + \boldsymbol{u}\cdot\boldsymbol{\nabla}\boldsymbol{u} = -\boldsymbol{\nabla}p + Pr\,\theta\boldsymbol{k} + Pr\nabla^2\boldsymbol{u}, \tag{3.2a, b}$$

and

$$\frac{\partial \theta}{\partial t} + \boldsymbol{u}\cdot\boldsymbol{\nabla}\theta = Rw + \nabla^2\theta, \tag{3.2c}$$

without approximation, where $R = \alpha(T_{-d} - T_0)gd^3/\kappa\nu$ (the Rayleigh number) and $Pr = \nu/\kappa$ (the Prandtl number).

Since we do not expect qualitative features of the chaotic regime to be greatly affected by the boundary conditions, we choose the simplest case of free, constant temperature boundaries and impose

$$\frac{\partial u}{\partial z} = \frac{\partial v}{\partial z} = w = 0, \quad \theta = 0 \quad \text{at } z = -1, 0. \tag{3.3}$$

The linear problem then has a simple analytic solution; the eigenfunctions are sinusoidal and provide a convenient basis for series expansions of solutions to the full nonlinear problem.

Following McLaughlin & Martin (1975), we impose a periodicity in the horizontal and take the Fourier representations

$$\boldsymbol{u}(x, y, z; t) = \mathrm{i} \sum_{lmn=-\infty}^{\infty} \boldsymbol{u}_{lmn}(t) \exp[\mathrm{i}(a_x lx + a_y my + \pi nz)], \tag{3.4a}$$

$$\theta(x, y, z; t) = \mathrm{i} \sum_{lmn=-\infty}^{\infty} \theta_{lmn}(t) \exp[\mathrm{i}(a_x lx + a_y my + \pi nz)], \tag{3.4b}$$

where the coefficients $\boldsymbol{u}_{lmn}(t) = (u_{lmn}(t), v_{lmn}(t), w_{lmn}(t))$ and $\theta_{lmn}(t)$ may vary with time. When these coefficients are constrained to take real values, the convection pattern is stationary. However when they are allowed to take complex values, the pattern may drift in the horizontal plane. Note that the imposition of periodicity is in effect a truncation procedure, replacing full Fourier transforms in the horizontal by Fourier series.

The boundary conditions (3.3) are satisfied when the Fourier coefficients obey the constraints

$$u_{lm-n} = u_{lmn}, \quad v_{lm-n} = v_{lmn}, \quad w_{lm-n} = -w_{lmn} \quad \theta_{lmn-n} = -\theta_{lmn}. \tag{3.5}$$

Also, the velocity and temperature fields must take real values, so

$$\boldsymbol{u}_{-l,-m,-n} = -\boldsymbol{u}^*_{l,m,n} \quad \theta_{-l,-m,-n} = -\theta^*_{l,m,n}, \tag{3.6}$$

where an asterisk superscript denotes a complex conjugate. Equations (3.5) and (3.6) may be used to reduce the range of the indices l, m, n to $0 \leqslant l, n < \infty$, $-\infty < m < \infty$. In addition, they imply that certain modes vanish:

$$\theta_{lm0} = w_{lm0} = \mathrm{Im}(\theta_{00n}) = \mathrm{Im}(w_{00n}) = 0, \quad \mathrm{Re}(u_{00n}) = \mathrm{Re}(v_{00n}) = 0. \tag{3.7}$$

Substitution of (3.4*a*) into the continuity equation (3.2*a*) gives

$$\pi n w_{lmn} = -a_x l u_{lmn} - a_y m v_{lmn}, \tag{3.8}$$

whence

$$u_{l00} = v_{0m0} = w_{00n} = 0 \quad (l, m, n \neq 0). \tag{3.9}$$

Substitution into the remainder of the perturbation equations (3.2) (cf. Hawkins 1984) yields the coupled set of nonlinear, ordinary differential equations:

$$\begin{aligned}\dot{u}_{lmn} = &-Pr\, K_{lmn}^2 u_{lmn} - Pr \frac{a_x l \pi n}{K_{lmn}^2} \theta_{lmn} \\ &+ \sum_{pqr} \left\{ \left[\frac{a_x (np - lr + n(l-p)\,\delta_{r,n})}{(n-r)} + a_x l A_{lmnpr} \right] u_{pqr}\, u_{l-p,\,m-q,\,n-r} \right. \\ &+ \left[\frac{a_y (nq - mr + n(m-q)\,\delta_{r,n})}{(n-r)} + a_x l B_{lmnpqr} \right] u_{pqr}\, v_{l-p,\,m-q,\,n-r} \\ &\left. + a_x l C_{lmnqr}\, u_{pqr}\, v_{l-p,\,m-q,\,n-r} \right\},\end{aligned} \tag{3.10a}$$

$$\begin{aligned}\dot{v}_{lmn} = &-Pr\, K_{lmn}^2 v_{lmn} - Pr \frac{a_y m \pi n}{K_{lmn}^2} \theta_{lmn} \\ &+ \sum_{pqr} \left\{ \left[\frac{a_y (nq - mr + n(m-q)\,\delta_{r,n})}{(n-r)} + a_y m C_{lmnqr} \right] v_{pqr}\, v_{l-p,\,m-q,\,n-r} \right. \\ &+ \left[\frac{a_x (np - lr + n(l-p)\,\delta_{r,n})}{(n-r)} + a_y m B_{lmnpqr} \right] v_{pqr}\, u_{l-p,\,m-q,\,n-r} \\ &\left. + a_y m A_{lmnpr}\, u_{pqr}\, u_{l-p,\,m-q,\,n-r} \right\},\end{aligned} \tag{3.10b}$$

$$\begin{aligned}\dot{\theta}_{lmn} = &-K_{lmn}^2 \theta_{lmn} - \frac{R}{\pi n} (a_x l u_{lmn} + a_y m v_{lmn}) \\ &- \sum_{pqr} \left\{ \left[\frac{a_x (np - lr - np\delta_{r,0})}{r} u_{pqr} + \frac{a_y (nq - mr - nq\delta_{r,0})}{r} v_{pqr} \right] \right. \\ &\left. \times \theta_{l-p,\,m-q,\,n-r} \right\} \quad (n \neq 0),\end{aligned} \tag{3.10c}$$

where the summation is over $-\infty < p, q, r < \infty$ and where

$$K_{lmn}^2 = a_x^2 l^2 + a_y^2 m^2 + \pi^2 n^2, \tag{3.11a}$$

$$A_{lmnpr} = \frac{a_x^2 (lr - np + np\delta_{r,0})(lr - np - n(l-p)\,\delta_{r,n})}{K_{lmn}^2\, r(n-r)}, \tag{3.11b}$$

$$B_{lmnpqr} = \frac{2 a_x a_y (lr - np + np\delta_{r,0})(mr - nq - n(m-q)\,\delta_{r,n})}{K_{lmn}^2\, r(n-r)}, \tag{3.11c}$$

$$C_{lmnqr} = \frac{a_y^2 (mr - nq + nq\delta_{r,0})(mr - nq - n(m-q)\,\delta_{r,n})}{K_{lmn}^2\, r(n-r)}. \tag{3.11d}$$

Equations (3.10) and (3.11) completely determine the velocity and temperature fields corresponding to a given initial state at $t = 0$, except for the contributions from the modes u_{000} and v_{000}. These may be shown to be constant in time and purely

imaginary (Hawkins 1984). They therefore describe a steady, uniform basic flow which we choose to set to zero.

A linear analysis of (3.10) shows that the mode (l, m, n) becomes unstable at a Rayleigh number

$$R_c(l, m, n) = \frac{(K^2_{lmn})^3}{K^2_{lm0}}, \tag{3.12}$$

in agreement with the standard analysis. The minimum value of $\frac{27}{4}n^4\pi^4$ is achieved when $K^2_{lm0} = \frac{1}{2}n^2\pi^2$. Thus the most unstable mode also has $n = 1$. Note that although the horizontal wavenumber of the most unstable mode is determined, the indices l and m, and the ratio $a_y : a_x$ are not.

The flow in the phase space $(u_{lmn}, v_{lmn}, \theta_{lmn})$ has negative divergence:

$$\sum_{lmn} \frac{\partial \dot{u}_{lmn}}{\partial u_{lmn}} + \frac{\partial \dot{v}_{lmn}}{\partial v_{lmn}} + \frac{\partial \dot{\theta}_{lmn}}{\partial \theta_{lmn}} = -(2Pr+1) \sum_{lmn} K^2_{lmn} < 0, \tag{3.13}$$

where the summation is over all allowed values of (l, m, n). Therefore the flow is contracting: when finite series are used, the set of attractors occupy zero volume in the phase space.

Finally, (3.10) and (3.11) are invariant under change of sign of all coefficients for which l is odd, of those for which m is odd, or of those for which n is odd. Thus the set of attractors in the phase space has a certain symmetry. In particular, when only a single attractor exists, the averages of products involving an odd number of such coefficients must be zero. This provides a useful check on the accuracy of numerical calculations of the statistical properties.

Expressions for the phase shift induced by the fluid, and the scattered intensity may now be found. It is consistent with the Boussinesq approximation of a linear variation of density with temperature, to assume a linear variation of refractive index also (cf. Hawkins 1984). Thus we take

$$n(T) = n_0[1 - \eta(T - T_{-d})]. \tag{3.14}$$

For water, $\eta_* = \eta R/(T_{*_{-d}} - T_{*_0}) \approx 1 \times 10^{-4}\ \mathrm{K}^{-1}$, and both η and ηR are small when R is large but $(T_{*_{-d}} - T_{*_0})$ not too large.

On substituting (3.1*b*) and (3.4*b*) into (3.14) and using $(T_{-d} - T_0) = R$, we find

$$n(x, y, z; t) = n_0[1 + \eta R(z+1) - \eta\theta(x, y, z; t)]. \tag{3.15}$$

Thus, from (2.11), the phase shift imposed by the fluid is

$$\phi(x_0, y_0; t) \approx k(n_0 - 1) + \tfrac{1}{2}kn_0\eta R - kn_0\eta R \sum_{lmn} \frac{[1-(-1)^n]}{\pi n} \theta_{lmn}(t) \times \exp[\mathrm{i}(a_x l x_0 + a_y m y_0)], \tag{3.16}$$

where the summation is over $-\infty < l, m, n < \infty$. Also, from (2.15)–(2.17), the intensity of light scattered by the fluid, relative to the incident intensity, is

$$I(x, y, z; t) \approx \Bigg| 1 + 4n_0\eta z \sum_{lmn} \Bigg\{ \frac{(a_x^2 l^2 + a_y^2 m^2)}{(2n+1)\pi} \theta_{l,m,2n+1}(t) \times \exp[\mathrm{i}(a_x l(x + \xi_x^s) + a_y m(y + \xi_y^s))] \Bigg\} + 8n_0^2\eta^2 z^2 \sum_{lmn} \sum_{pqr} \Bigg\{ \frac{a_x^2 a_y^2 (lq - mp)^2}{(2n+1)(2r+1)\pi^2} \theta_{l,m,2n+1}(t)\, \theta_{p,q,2r+1}(t) \times \exp[\mathrm{i}(a_x(l+p)(x + \xi_x^s) + a_y(m+q)(y + \xi_y^s))] \Bigg\} \Bigg|^{-1}, \tag{3.17}$$

where

$$\xi_x^s = 4n_0\eta z \sum_{lmn} \frac{\mathrm{i}a_x l}{(2n+1)\pi}\theta_{l,m,2n+1}(t)\exp\left[\mathrm{i}(a_x l(x+\xi_x^s)+a_y m(y+\xi_y^s))\right], \quad (3.18)$$

and

$$\xi_y^s = 4n_0\eta z \sum_{lmn} \frac{\mathrm{i}a_y m}{(2n+1)\pi}\theta_{l,m,2n+1}(t)\exp\left[\mathrm{i}(a_x l(x+\xi_x^s)+a_y m(y+\xi_y^s))\right], \quad (3.19)$$

and where the summations are over $-\infty < l, m, n, p, q, r < \infty$. Only modes θ_{lmn} where n is odd contribute to the phase screen and the intensity: those with n even average to zero in the vertical.

4. The Lorenz model

The well-known Lorenz model is obtained by applying the truncation $|l| \leqslant 1$, $m = 0$, $|l|+|n| \leqslant 2$ (or equivalently $m = 0$, $l^2+n^2 \leqslant 4$) to the series. It is the most severe truncation to retain nonlinear terms, and involves just three coefficients: X, Y and Z in the notation of Lorenz (1963).

The velocity field $\boldsymbol{u}(x,z;t) = (u(x,z;t), 0, w(x,z;t))$ takes the form

$$u(x,z;t) = -4u_{101}(t)\sin(a_x x)\cos(\pi z),$$

$$w(x,z;t) = 4(a_x/\pi)u_{101}(t)\cos(a_x x)\sin(\pi z),$$

and the temperature perturbations

$$\theta(x,z;t) = -4\theta_{101}(t)\cos(a_x x)\sin(\pi z) - 2\theta_{002}(t)\sin(2\pi z). \quad (4.1)$$

This forms a stationary convection pattern of two-dimensional roll cells.

A ray of light with normal incidence travels through the fluid along the path

$$x(z;t) = x_0 + \frac{4\eta a_x}{\pi^2}\theta_{101}(t)\sin(a_x x_0)[\pi(z+1)+\sin(\pi z)] + O(\eta^2), \quad (4.2)$$

and the phase difference between light leaving and entering the fluid is

$$\phi(x_0;t) = k(n_0 - 1 + \tfrac{1}{2}n_0\eta R) - \frac{8kn_0\eta}{\pi}\theta_{101}(t)\cos(a_x x_0) + O(\eta^2). \quad (4.3)$$

An exact expression may be found for the intensity (Hawkins 1984):

$$I(x,z;t) = 1 + 2\sum_{l=1}^{\infty}(\sigma(l))^l \cos(la_x x) J_l(\omega), \quad (4.4)$$

where

$$\omega = \frac{-8kn_0\eta}{\pi}\theta_{101}(t)\left|\sin\left(\frac{la_x^2 z}{2k}\right)\right|, \quad (4.5)$$

and

$$\sigma(l) = \mathrm{sgn}\left(\sin\left(\frac{la_x^2 z}{2k}\right)\right), \quad \sigma(0) = 1. \quad (4.6)$$

In the pre-caustic region

$$\left|z\frac{8n_0\eta a_x^2}{\pi}\theta_{101}(t)\cos(a_x(x+\xi_x^s))\right| < 1, \quad (4.7)$$

the geometrical optics approximation of the intensity field is

$$I(x,z;t) \sim \left|1 + z\frac{8n_0\eta a_x^2}{\pi}\theta_{101}(t)\cos(a_x(x+\xi_x^s))\right|^{-1} \quad \text{as } k\to\infty, \quad (4.8)$$

where
$$a_x \xi_x^s = -z\frac{8n_0\eta a_x^2}{\pi}\theta_{101}(t)\sin(a_x(x+\xi_x^s)). \tag{4.9}$$

It is convenient to introduce the variables

$$b = \frac{4\pi^2}{(a_x^2+\pi^2)}, \quad R_c = \frac{(a_x^2+\pi^2)^3}{a_x^2}, \quad r = \frac{R}{R_c}, \tag{4.10}$$

and
$$\left.\begin{aligned} t' &= (a_x^2+\pi^2)t, \quad X = \frac{-2\sqrt{2}a_x u_{101}}{(a_x^2+\pi^2)}, \\ Y &= \frac{2\sqrt{2}a_x^2\theta_{101}}{(a_x^2+\pi^2)^3}, \quad Z = \frac{2a_x^2\theta_{002}}{(a_x^2+\pi^2)^3}. \end{aligned}\right\} \tag{4.11}$$

Then the time evolution of X, Y and Z is governed by the coupled system of equations

$$\dot{X} = -Pr\,X + Pr\,Y, \quad \dot{Y} = rX - Y - ZX, \quad \dot{Z} = -bZ + XY, \tag{4.12}$$

where a 'dot' denotes differentiation with respect to the dimensionless time t'.

Many basic properties of these equations are now well-known, and may be found in the paper by Lorenz (1963), and the book by Sparrow (1982). Some averages and correlation functions in the chaotic regime have also been calculated by Lücke (1976), Knobloch (1978), and Grossmann & Sonneborn-Schmick (1982). We present further numerical results of statistical properties (in particular probability density functions and autocorrelations of X^2, Y^2 and Z^2), and discuss the statistical properties of the scattered light field. First, however, we outline the basic properties of the equations which are relevant to the discussion of their statistical properties.

Equations (4.12) are invariant under the transformation $(X, Y, Z) \to (-X, -Y, Z)$. All solutions to the equations may be shown to be bounded, and the flow in the phase space (X, Y, Z) is contracting. There are three fixed points of (4.12). The first, at the origin, exists for all values of r; it is stable when $r < 1$ and unstable when $r > 1$. The remaining two, $X = Y = \pm(b(r-1))^{\frac{1}{2}}$, $Z = (r-1)$ exist only when $r \geqslant 1$; they are stable when $r < r_c = Pr(Pr+b+3)/(Pr-b-1)$ and unstable otherwise. When r exceeds the critical value r_c, a wide variety of behaviour is observed depending upon the values of all three parameters. The orbits may be periodic, quasi-periodic or chaotic. We choose to study chaotic solutions.

We have used two sets of parameters, $(Pr, b, r) = (10, \frac{8}{3}, 28)$ and $(Pr, b, r) = (10, \frac{8}{3}, 175)$, both of which generate chaotic solutions. Typical time series are shown in figure 2.

We first note the apparent symmetry, about the origin, in the time series of X and Y. We therefore expect averages of the form $\langle X^l Y^m Z^n \rangle$, where l, m and n are integers, to vanish when $(l+m)$ is odd. The series are dominated by a spiralling motion about the non-zero fixed points, together with a switching between the points. Although there is no well-defined period for these characteristics, we may associate a typical timescale with each. At $r = 28$, a typical time for one cycle about a fixed point is $\tau_c \approx 0.75$, whilst a typical time for switching between the fixed points is $\tau_s \approx 4$. At $r = 175$, the switching occurs much more rapidly, presumably because the fixed points are more strongly repelling, and $\tau_s \approx 2\tau_c$. The overall motion is faster, with $\tau_c \approx 0.25$, and the amplitudes are greater (note the different scales). The spectra are not shown, but all have broadband noise typical of chaos, with very weak 'peaks' at the frequencies corresponding to the timescales τ_c.

On the grounds of numerical evidence, the Lorenz attractor is thought to be

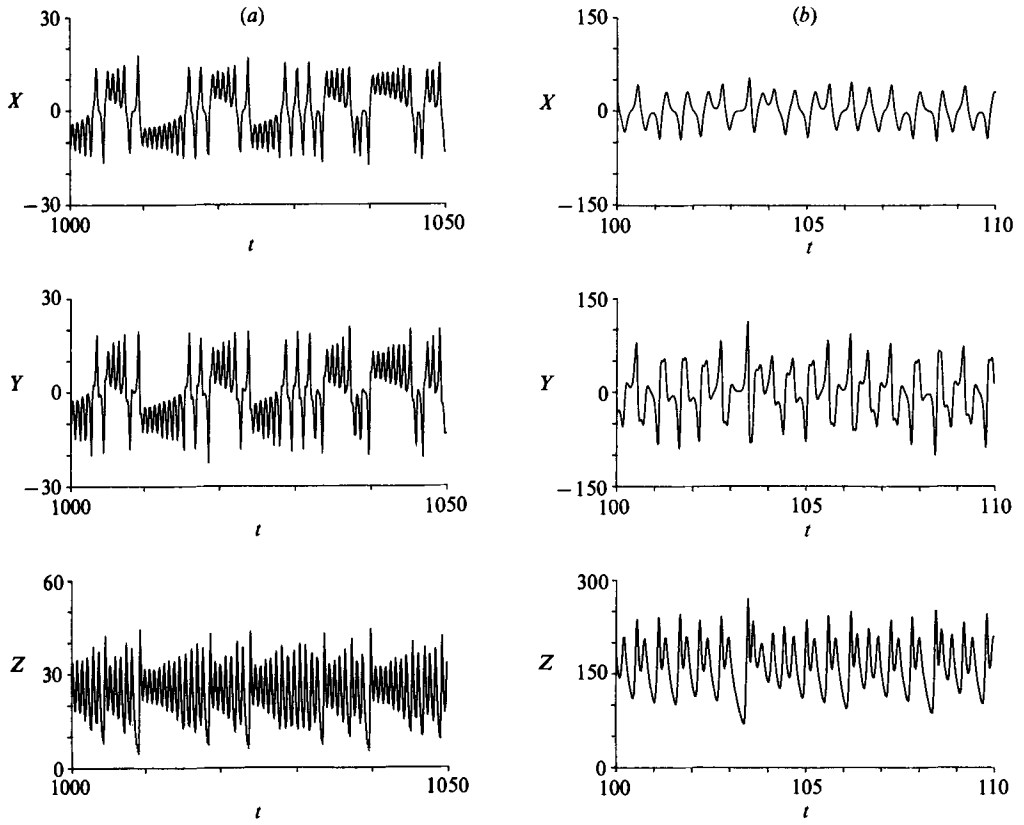

FIGURE 2. Time series for the Lorenz model with (*a*) $r = 28$, $Pr = 10$ and $b = \frac{8}{3}$; (*b*) $r = 175$, $Pr = 10$ and $b = \frac{8}{3}$.

ergodic and statistically stationary (Knobloch 1978). We assume this to be so and use time averages, which we denote by angular brackets:

$$\langle f(t_0)\rangle = \lim_{T\to\infty} \frac{1}{T}\int_0^T f(t+t_0)\,\mathrm{d}t, \tag{4.13}$$

where stationarity ensures the result is independent of t_0. The average of the time-derivative of a bounded function vanishes:

$$\langle \dot{f}\rangle = \lim_{T\to\infty} \frac{f(T)-f(0)}{T} = 0. \tag{4.14}$$

Since the Lorenz attractor is bounded, this yields relationships between averages:

$$\begin{aligned} n\langle l+1, m+1, n-1\rangle - m\langle l+1, m-1, n+1\rangle &= (Pr\,l+m+bn)\langle l, m, n\rangle \\ &\quad - Pr\,l\langle l-1, m+1, n\rangle - rm\langle l+1, m-1, n\rangle, \end{aligned} \tag{4.15}$$

where $\langle l, m, n\rangle = \langle X^l Y^m Z^n\rangle$ (Hawkins 1984). Similar relationships may be found between correlation functions (Hawkins 1984).

We turn now to the numerical results. Equations (4.12) were integrated using a Runge–Kutta–Merson method, with a tolerance level of 10^{-6}. The points $(X(t), Y(t), Z(t))$ were calculated for $0 < t < 4000$, at intervals of 0.125 at $r = 28$ and

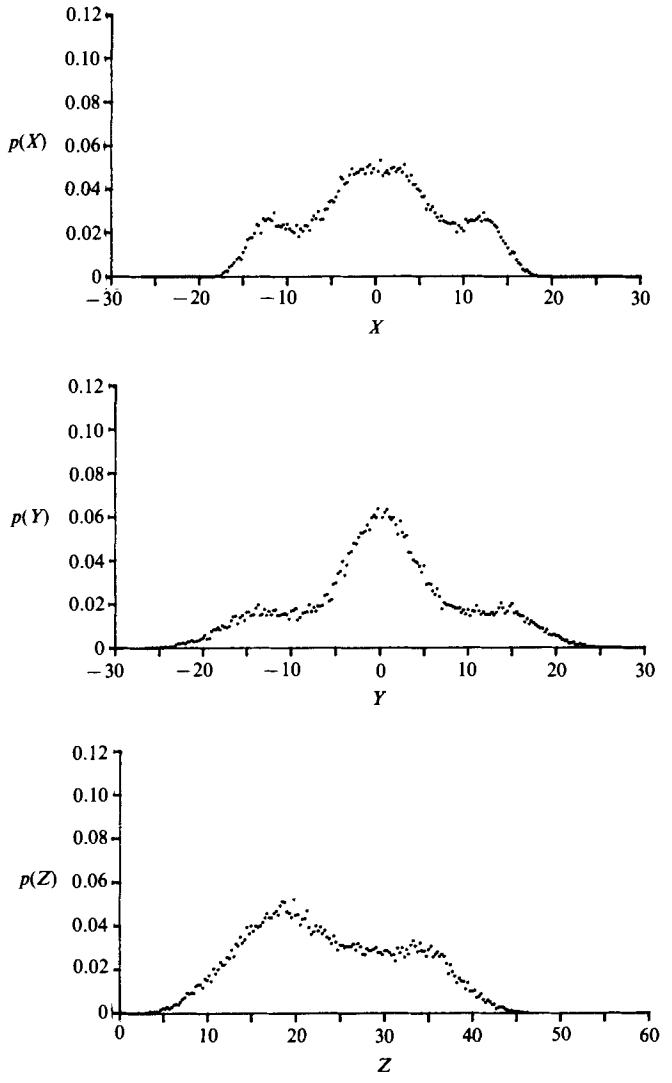

FIGURE 3. Probability density functions of X, Y and Z of the Lorenz model with $r = 28$, $Pr = 10$ and $b = \frac{8}{3}$.

0.01 at $r = 175$. Points for which $t < 500$ were discarded in order to eliminate initial transients.

The probability density functions are shown in figures 3 and 4: they were computed by counting the number of points to fall within bins of size 0.25 for $r = 28$, and 0.2 for $r = 175$. A bin giving a value of $p = 0.01$ contains 80 samples at $r = 28$, and 8000 at $r = 175$. The graphs are qualitatively similar, although there are more peaks, and these are sharper, at the higher value of r. The scatter in the diagrams is caused by the series having many turning points, very finely spaced in X (or Y or Z as appropriate), which produce peaks or (integrable) singularities in the probability density functions.

The autocorrelation functions of X, Y and Z, and of X^2, Y^2 and Z^2 are shown in figures 5 and 6. Those of X, Y and Z agree qualitatively with those computed by Lücke (1976) and Grossmann & Sonneborn-Schmick (1982). Those of X and Y are

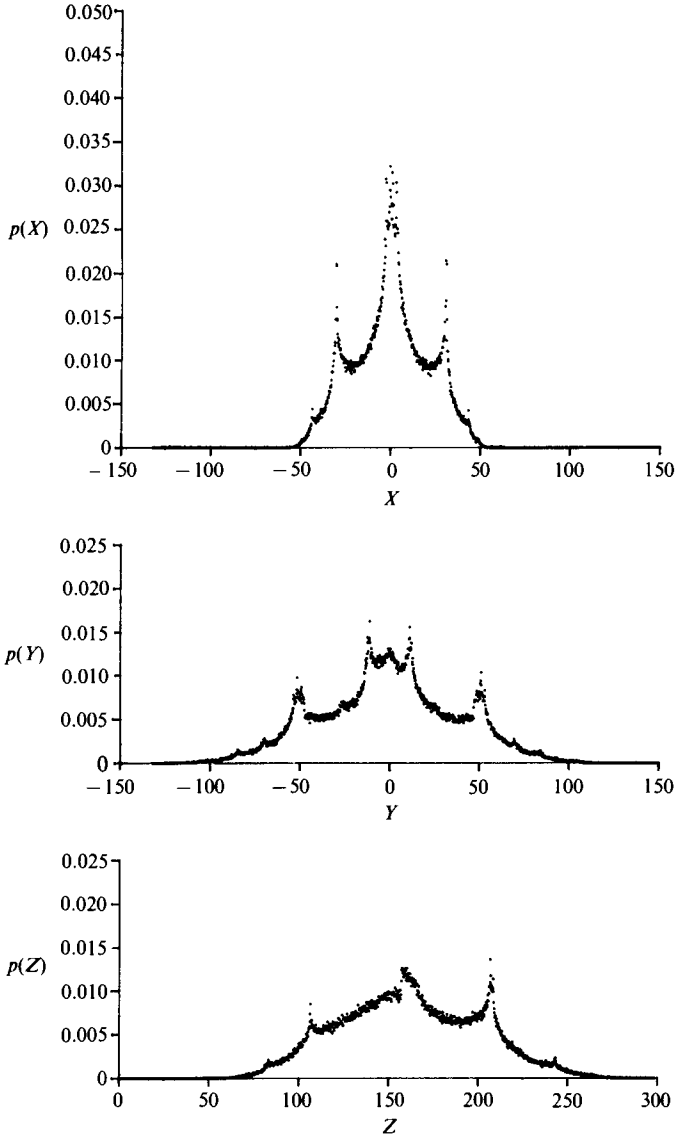

FIGURE 4. Probability density functions of X, Y and Z of the Lorenz model with $r = 175$, $Pr = 10$ and $b = \frac{8}{3}$.

very similar: both have a rapid decay, followed by oscillations which are more pronounced at the higher value of r. The timescale of the initial rapid decay is of order 0.5 at $r = 28$ and 0.1 at $r = 175$. The timescale, τ_c, characterizing one cycle around a fixed point appears to be associated with the first peak of the correlation function, or possibly the zero that occurs just before it (Grossmann & Sonneborn-Schmick 1982). The autocorrelation functions of Z show a much slower decay, with regular oscillations. We may distinguish a timescale of 0.8 at $r = 28$, corresponding to τ_c, and of both $\tau_c \approx 0.25$ and $\tau_s \approx 0.55$ at $r = 175$.

The autocorrelations of X^2, Y^2 and Z^2 are similar to one another, all showing the regular oscillations seen in that of Z (although at $r = 175$, the autocorrelation function of Y^2 has much weaker oscillations than that of X^2 or of Z^2). The difference

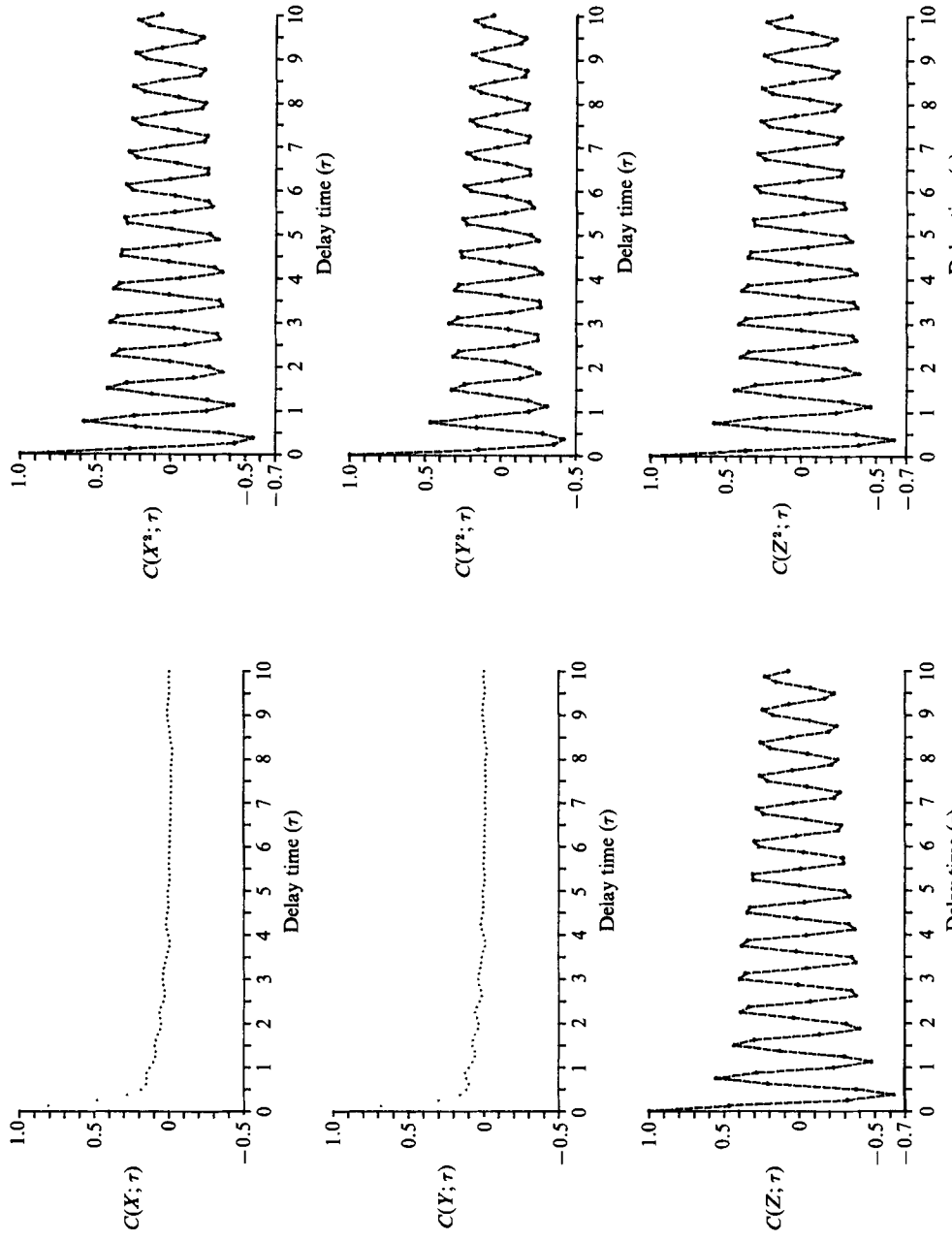

FIGURE 5. Autocorrelation functions of X, Y and Z and of X^2, Y^2 and Z^2, with $r = 28$, $Pr = 10$ and $b = \frac{8}{3}$.

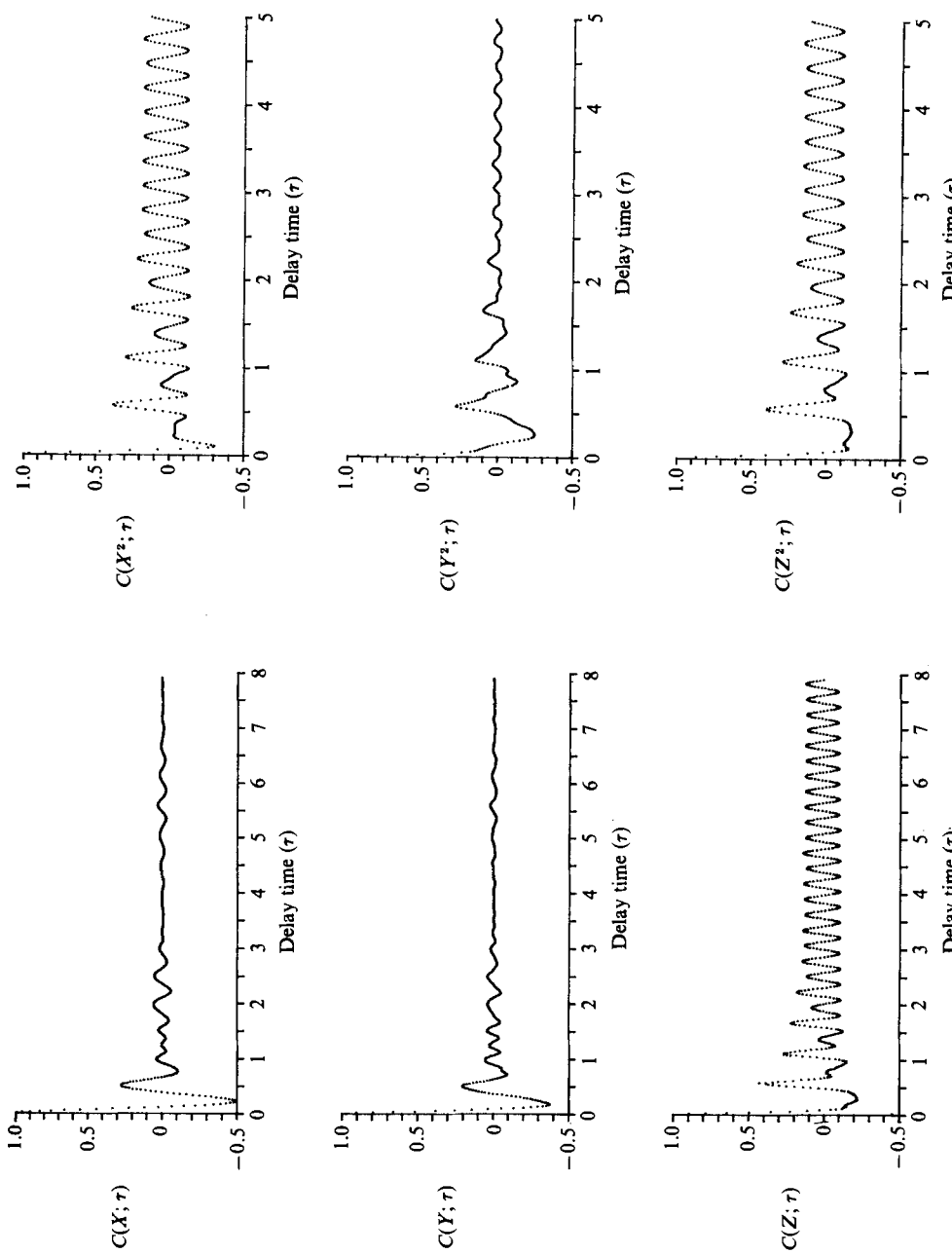

FIGURE 6. Autocorrelation functions of X, Y and Z and of X^2, Y^2 and Z^2, with $r = 175$, $Pr = 10$ and $b = \frac{8}{3}$.

between the autocorrelation functions of X and X^2 may easily be understood. The switching between the two fixed points destroys the correlation in X, but is ineffective in that of X^2 since the two fixed points are then indistinguishable.

The resemblance between the autocorrelation functions of X^2 and of Z is striking. Integral relationships between the two may be found:

$$\langle X_0^2 X_\tau^2\rangle = 4Pr^2\langle Z_0 Z_\tau\rangle - 4Pr^2(Pr-b)\int_0^\infty [\langle Z_0 Z_{\tau+s}\rangle + \langle Z_0 Z_{\tau-s}\rangle]\, e^{-2Prs}\, ds$$
$$-4Pr^2(2Pr-b)^2\int_0^\infty\int_0^\infty \langle Z_0 Z_{\tau-s+u}\rangle\, e^{-2Pr(s+u)}\, ds\, du, \quad (4.16)$$

and

$$4Pr^2\langle Z_0 Z_\tau\rangle = \langle X_0^2 X_\tau^2\rangle + (2Pr-b)\int_0^\infty [\langle X_0^2 X_{\tau+s}^2\rangle + \langle X_0^2 X_{\tau-s}^2\rangle]\, e^{-bs}\, ds$$
$$+(2Pr-b)^2\int_0^\infty\int_0^\infty \langle X_0^2 X_{\tau+s-u}^2\rangle\, e^{-b(s+u)}\, ds\, du, \quad (4.17)$$

(Hawkins 1984). However, we have been unable to find an explicit relationship.

We turn now to discuss the scattered light field, and its statistical properties. Since the phase shift is directly proportional to $Y(t)$ (through $\theta_{101}(t)$, equations (4.3) and (4.11)), its statistical properties are identical to those of Y when scaled by the appropriate factor.

The intensity is more complicated. We confine our attention to the pre-caustic region, and use (4.7) to estimate its size. Taking $|Y| < 30$, $n_0 = 1.333$ and $\eta = 6.06\times10^{-9}$ for water, we find that caustics are never formed in the region $z < 1400$, in dimensionless units. Thus for 36.4 K temperature difference across 1 cm of water, $z_* < 14$ m. Obviously the phase screens produced by real experiments will be more complicated than the simple sinusoid produced by the Lorenz model. Since the maximum value of z scales inversely with the curvature of the screen, the presence of smaller scales will bring the caustics closer to the fluid. However, the result does indicate that we should expect the pre-caustic region to extend sufficiently far from the fluid for measurements to be made within it. We may define a characteristic length of the pre-caustic region, from (4.7) and (4.11), as $z_c = \pi/(2\sqrt{2}n_0\eta R_c a_x^2)$. This is the closest to the screen that caustics may be formed when $Y(t) = 1$. Henceforth we will use the renormalized value of z, $z' = z/z_c$.

In addition to the periodicity of wavelength $2\pi/a_x$ in the horizontal, the intensity field obeys the symmetries

$$I\left(\frac{\pi}{a_x}+x, z'; t\right) = I\left(\frac{\pi}{a_x}-x, z'; t\right), \quad (4.18)$$

and

$$I(x, z'; t: Y(t) = -Y') = I\left(\frac{\pi}{a_x}-x, z'; t: Y(t) = +Y'\right). \quad (4.19)$$

Therefore we restrict our attention to the domain $x\in[0, \pi/2a_x]$.

The variation of intensity with $z'Y$ is shown in figure 7, for different values of x. The mapping may be two to one at all values of x when $z'Y$ is allowed to take all values in the range $[-1, 1]$. However, within the pre-caustic region, the range of possible values is less than this; thus at points near $x = n\pi/a_x$ the mapping becomes one to one. The boundary of this region is shown in figure 8 (see Hawkins (1984) for detailed calculations). Its shape is important in the application of theory to experiment, since we would ideally like to take measurements in a region where the

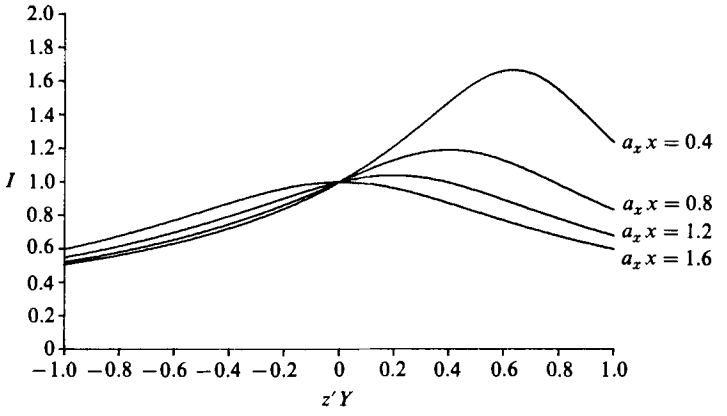

FIGURE 7. Plot of I versus $z'Y$.

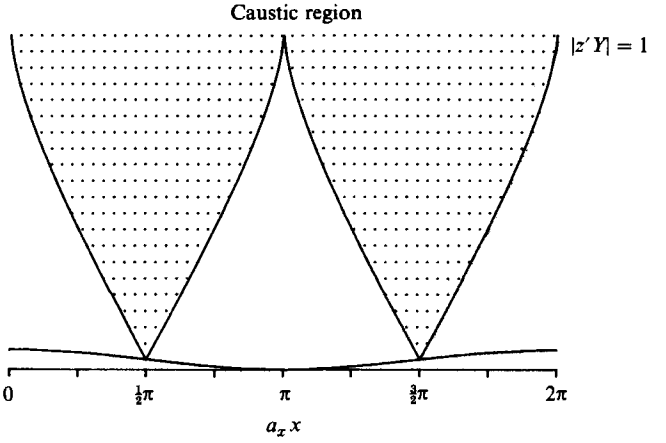

FIGURE 8. The single-valued region (unshaded) of the mapping $z'Y \to I$.

intensity is a single-valued function of the temperature field. In a real fluid, the contributions of additional modes to the phase screen must complicate the shape of the region, and any movement of the convection pattern may cause it to distort with time. Therefore, there may be no points at which the intensity field has the desired properties. Moreover, if such points did, by chance, exist, it may prove impossible to identify them in practice.

The first six normalized intensity moments, $\langle I^m \rangle / \langle I \rangle^m$, were calculated for each of $z' = 0.01$ and 0.025. It was found that at the lower value there was insufficient contrast to distinguish them from the values

$$\frac{\langle I^m \rangle}{\langle I \rangle^m} - 1 = \tfrac{1}{2} m(m-1)\left[\frac{\langle I^2 \rangle}{\langle I \rangle^2} - 1\right], \tag{4.20}$$

which hold regardless of the form of I, provided its variance is small (cf. Hawkins 1984). At the higher value, there is a significant deviation from this relationship, as shown in figure 9. However, for this value of z' we are closer to the caustic region than to the fluid, and the intensity is a single-valued function of intensity over only a small horizontal extent.

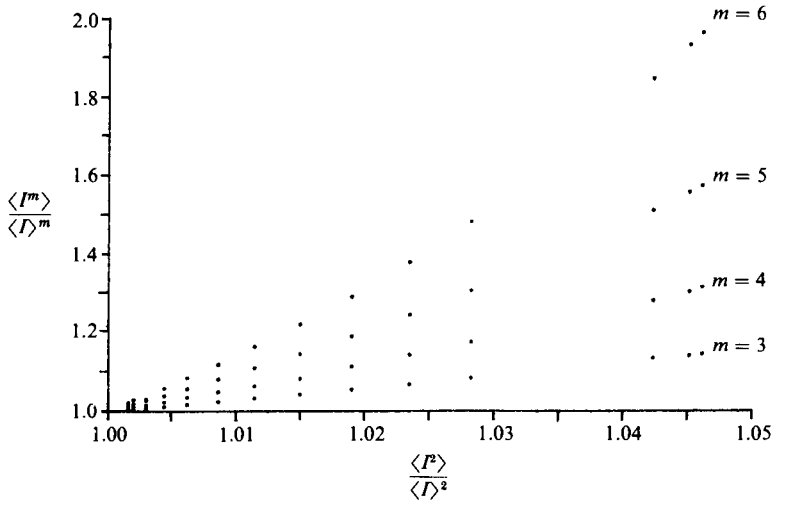

FIGURE 9. Normalized moments $\langle I^m\rangle/\langle I\rangle^m$, for $m = 3, 4, 5$ and 6, versus $\langle I^2\rangle/\langle I\rangle^2$ for $r = 28$, $Pr = 10$, $b = \frac{8}{3}$ and $z' = 0.025$.

Thus we have a dilemma between choosing z' to be large enough that the intensity moments differ from the universal relationship (4.20), but not too close to the caustic region.

The importance of remaining within the single-valued region may be further illustrated by studying the probability density functions of the intensity for different horizontal positions. Those for $z' = 0.025$ are shown in figure 10. Assuming $|Y(t)| \leqslant 30$, then the intensity is a single-valued function of $Y(t)$ when $0 \leqslant a_x x \leqslant 0.23$. Within this single-valued region, the probability density function of the intensity,

$$p_I(I_0) = \sum_{i:I(Y_i)=I_0} \left[p_Y(Y_i) \frac{\mathrm{d}Y}{\mathrm{d}I}\bigg|_{Y_i} \right], \tag{4.1}$$

is similar to that of Y, but increasingly stretched and flattened as I increases. Outside this region, however, two distinct values of Y contribute to $p_I(I)$ at the higher values of I. Thus the distribution of the intensity there is produced not only by the stretching described above, but also a folding at the upper end, and many qualitative features of $p_Y(Y)$ are destroyed.

The normalized correlation functions of the intensity

$$C(\tau; a_x x) = \frac{\langle I(a_x x; t)\, I(a_x x; t+\tau)\rangle - \langle I\rangle^2}{\langle I^2\rangle - \langle I\rangle^2}, \tag{4.22}$$

are shown in figure 11, for $z' = 0.025$. Qualitatively similar results were found at $z' = 0.01$. When $a_x x \leqslant 0.8$, there is an initial rapid decay followed by very weak oscillations; $R(\tau; a_x x)$ is very similar to the autocorrelation function of Y shown in figure 5. When $a_x x \geqslant 1.2$, however, $R(\tau; a_x x)$ is highly oscillatory and qualitatively similar to the autocorrelation function of Y^2 shown in figure 5. This may be understood by noting from figure 7 that when $a_x x \geqslant 1.2$ the intensity is almost symmetric with respect to Y. Thus taking $a_x x$ near the value $\frac{1}{2}\pi$ destroys the distinction between positive and negative values of Y in the same way as squaring Y.

Even for the simple Lorenz model, then, the behaviour of the statistical properties of the intensity is complex, and varies with position. The phase shift, however, is

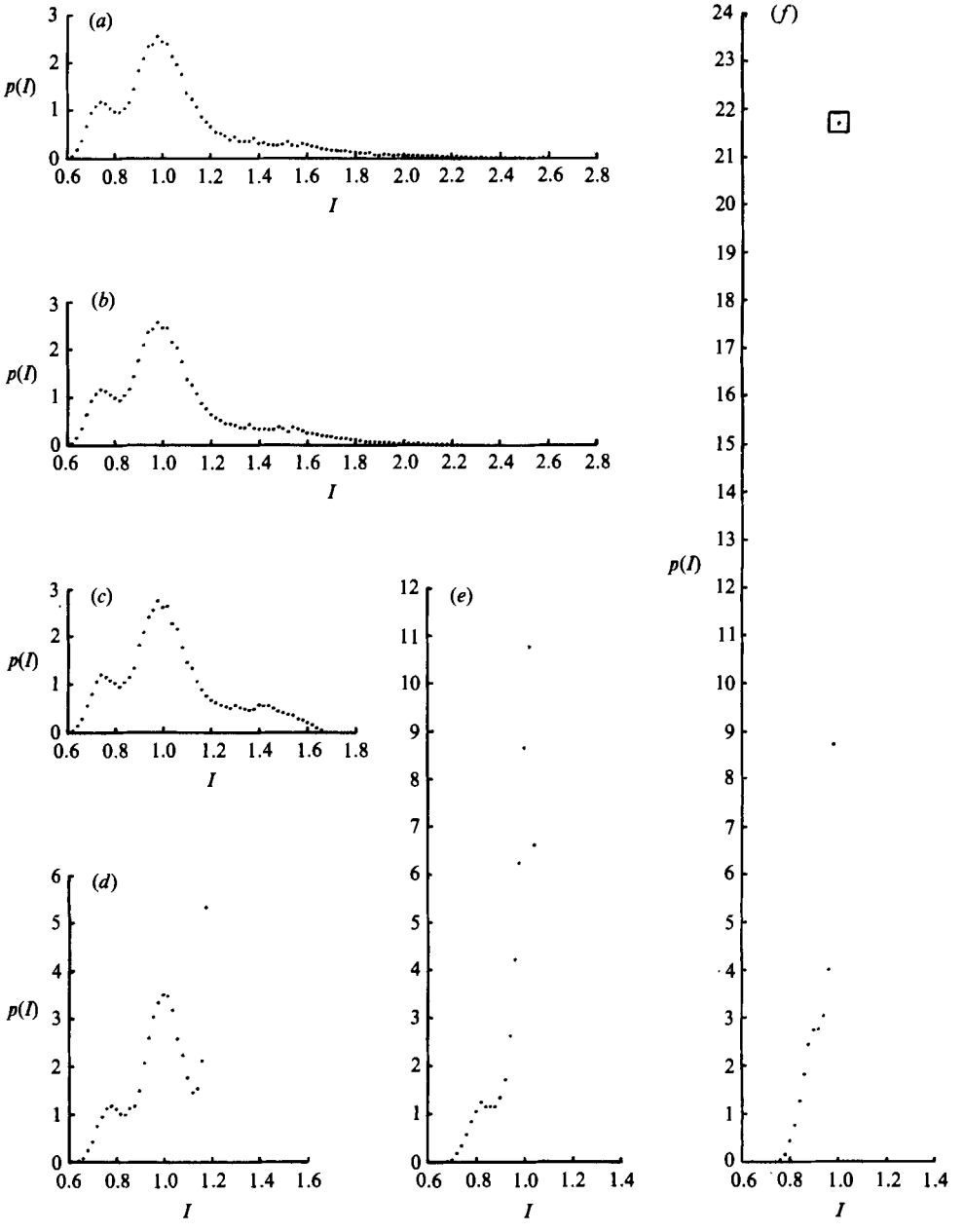

FIGURE 10. Probability density functions of the intensity for $r = 28$, $Pr = 10$, $b = \frac{8}{3}$ and $z' = 0.025$ at (*a*) $a_x x = 0$; (*b*)$a_x x = 0.2$; (*c*) $a_x x = 0.4$; (*d*) $a_x x = 0.8$; (*e*) $a_x x = 1.2$; (*f*) $a_x x = 1.6$.

directly proportional to the average of the temperature field taken vertically through the fluid. Thus its statistical properties are more closely related to those of the temperature field, and provide a more sensitive indication of the latter. Also, the phase is easier to calculate from mathematical models, and avoids the problem in experiments of distinguishing between the pre-caustic and caustic regions. We suggest, then, that it is the more useful quantity to measure, and will henceforth confine our attention to it rather than the intensity.

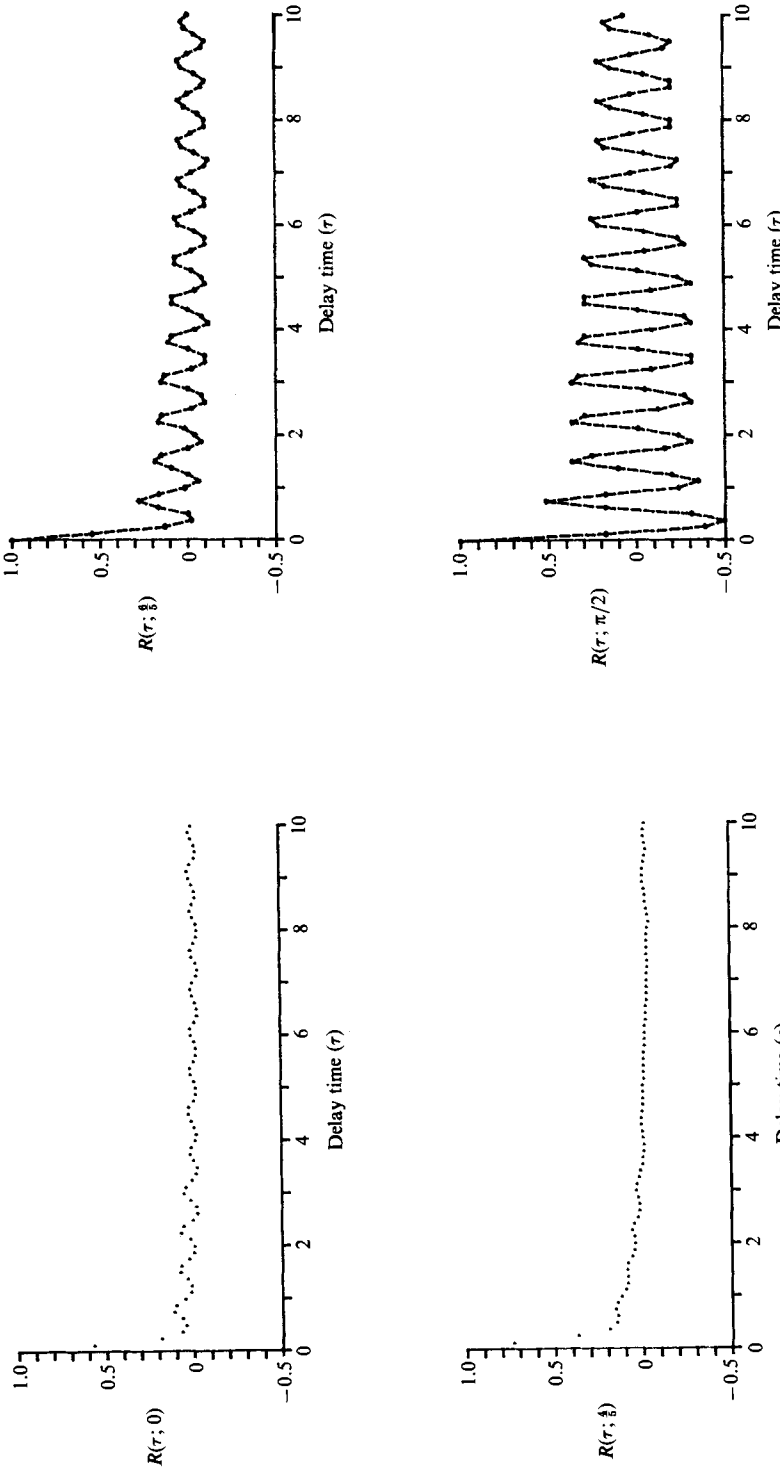

FIGURE 11. Autocorrelation functions of the intensity for $r = 28$, $Pr = 10$, $b = \frac{8}{3}$ and $z' = 0.025$.

5. A higher-order model

A higher-order model, obtained by adopting the truncation $|l| \leqslant 2$, $m = 0$, $|l|+|n| \leqslant 3$ and requiring all coefficients to be real, has also been investigated. This model involves nine coefficients (u_{101}, u_{102}, u_{201}, θ_{001}, θ_{002}, θ_{003}, θ_{101}, θ_{102}, θ_{201}).

For convenience, we make the transformations

$$u_{lmn} \to \frac{3a_x}{(a_x^2+\pi^2)} u_{lmn}, \quad \theta_{lmn} \to \frac{3\pi a_x^2}{(a_x^2+\pi^2)^3} \theta_{lmn}, \quad t \to (a_x^2+\pi^2)\, t, \tag{5.1}$$

and define

$$b = \frac{\pi^2}{(a_x^2+\pi^2)}, \quad R_c = \frac{(a_x^2+\pi^2)^3}{a_x^2}, \quad r = \frac{R}{R_c}. \tag{5.2}$$

Note the slightly different scaling of b and of the Fourier coefficients from that used in the Lorenz model. Then the equations governing the time-evolution of the coefficients of the nine-mode system are:

$$\begin{aligned}
\dot{u}_{101} &= -Pr\, u_{101} - Pr\, \theta_{101} + 3(\tfrac{1}{2}-b)\, u_{102}\, u_{201}, \\
\dot{u}_{102} &= -Pr\,(1+3b)\, u_{102} - \frac{2Pr}{(1+3b)} \theta_{102} - \frac{6(1-b)}{(1+3b)} u_{101}\, u_{201}, \\
\dot{u}_{201} &= -Pr\,(4-3b)\, u_{201} - \frac{2Pr}{(4-3b)} \theta_{201} + \frac{3b}{2(4-3b)} u_{101}\, u_{102}, \\
\dot{\theta}_{001} &= -b\theta_{001} + \tfrac{1}{3}(2u_{101}\, \theta_{102} + u_{102}\, \theta_{101}), \\
\dot{\theta}_{002} &= -4b\theta_{002} - \tfrac{4}{3}(u_{101}\, \theta_{101} + 2u_{201}\, \theta_{201}), \\
\dot{\theta}_{003} &= -9b\theta_{003} - (2u_{101}\, \theta_{102} + u_{102}\, \theta_{101}), \\
\dot{\theta}_{101} &= -\theta_{101} - ru_{101} + \tfrac{1}{6}(3u_{102}\, \theta_{003} + 4u_{101}\, \theta_{002} + 6u_{201}\, \theta_{102} + 3u_{102}\, \theta_{201} - u_{102}\, \theta_{001}), \\
\dot{\theta}_{102} &= -(1+3b)\, \theta_{102} - \tfrac{1}{2} ru_{102} + \tfrac{1}{3}(3u_{101}\, \theta_{003} - 3u_{101}\, \theta_{201} - u_{101}\, \theta_{001} - 3u_{201}\, \theta_{101}),
\end{aligned}$$

and

$$\dot{\theta}_{201} = -(4-3\mathrm{b})\, \theta_{201} - 2ru_{201} + \tfrac{1}{6}(6u_{101}\, \theta_{102} + 8u_{201}\, \theta_{002} - 3u_{102}\, \theta_{101}). \tag{5.3}$$

We have identified four fixed points, in addition to the origin: the pair with non-zero coefficients

$$\theta_{101} = -u_{101} = \pm 3[\tfrac{1}{2}b(r-1)]^{\frac{1}{2}}, \quad \theta_{002} = \tfrac{3}{2}(r-1) \quad (r \geqslant 1), \tag{5.4}$$

and the pair with non-zero coefficients

$$\begin{aligned}
\theta_{201} &= -\tfrac{1}{2}(4-3b)^2 u_{201} = \pm\tfrac{1}{2}.3(4-3b)[\tfrac{1}{2}b(r-\tfrac{1}{4}(4-3b)^3)]^{\frac{1}{2}}, \\
\theta_{002} &= \tfrac{3}{2}[r-\tfrac{1}{4}(4-3b)^3] \quad (r \geqslant \tfrac{1}{4}(4-3b)^3),
\end{aligned} \tag{5.5}$$

The origin is linearly stable when $r < \min(1, \frac{1}{4}(4-3b)^3, (1+3b)^3)$. Note that r is defined such that the modes $(1,0,1)$ are assumed to be the most stable. The apparent paradox of instability at $r < 1$ when $b > \frac{1}{3}(4-4^{\frac{1}{3}})$ arises because the wavenumber a_x is then such that the modes $(2,0,1)$ are the most unstable. On redefining $r' = R/R_c'$, where the critical Rayleigh number is now $R_c' = (4a_x^2+\pi^2)^3/4a_x^2$, the criterion for stability of the system, $r' < 1$ is recovered.

We have investigated numerically the stability of the four non-trivial fixed points for $Pr = 10$ and $b = \frac{2}{3}$. The results are consistent with the pair (5.4) being stable when

$r < r_c = Pr(Pr+4b+3)/(Pr-4b-1)$, as in the Lorenz model; the pair (5.5) are stable when $r < 9.9$.

The behaviour of the system over the interval $25 \leqslant r \leqslant 35$ has been investigated numerically. Unlike the Lorenz system, which behaves chaotically throughout this interval, we find the nine-mode system has a quasi-periodic solution at $r = 26.4$, and a periodic solution at $r = 35$, with chaos occurring only over the narrow range $25 \leqslant r < 26.3$. Some spectra of the mode $u_{101}(t)$ are shown in figure 12.

We have investigated the statistical properties of the system for the parameter values $r = 26$, $Pr = 10$ and $b = \frac{2}{3}$. The system was integrated numerically over 20000 time units, with values of all nine coefficients taken at intervals of 0.05 time units and stored in binary format. The integration took 13 hours of CPU time on an ICL 2980, and the orbit occupied 21 Megabytes of storage space.

A typical portion of the time series of each coefficient is shown in figure 13. There appears to be an alternation between motion near the 'Lorenz attractor', and motion near an unstable limit cycle. Although the six extra modes introduced in this model all have much smaller amplitudes than the three 'Lorenz modes', they have significantly altered the behaviour of the latter.

The statistical properties of this system have proved more difficult to find than those of the Lorenz system. Convergence of the statistical properties of the 'Lorenz modes' u_{101}, θ_{101} and θ_{002} was satisfactory, but convergence of these properties of the remaining six modes was weak. This result is disturbing. In real time, the length of the series is nearly eleven days: to maintain steady external conditions in any experiment over such a time would prove extremely difficult. However, since satisfactory convergence was observed at much shorter times in the Lorenz system we might hope the nine-mode system is atypical in some way. It was not thought to be appropriate to generate even longer time series of this model; the weak convergence should be borne in mind in the following discussion of the results.

The probability density functions are shown in figure 14. The most noticeable difference between those of the modes u_{101}, θ_{101} and θ_{002} obtained from this system and those obtained from the Lorenz system, is the pronounced dip near the origin. Other qualitative features such as the side peaks, the scatter caused by the extrema of the orbit, and the symmetry about the origin, are preserved.

The autocorrelation functions of the modes are shown in figure 15. We may distinguish a timescale $\tau \approx 0.7$ for the rapid oscillations, one of $\tau \approx 8$ for the slower oscillations of the amplitude, and one of $\tau \approx 12$ for the slow decay in those of u_{101} and θ_{101}. The first two timescales correspond respectively to those of the rapid fluctuations and of the change in amplitude in the time series. The origin of the longer timescale is not clear. Corresponding velocity and temperature modes have qualitatively similar autocorrelation functions in the same way as do X and Y in the Lorenz system. The apparent residual correlation in the autocorrelation functions of u_{102}, u_{201}, θ_{001} and θ_{201} may be due to lack of convergence, but might also be a real effect and should not be dismissed.

The autocorrelation functions of the squares of the modes are shown in figure 16. In analogy to the behaviour of the Lorenz system, the autocorrelation functions of u_{101}^2, θ_{101}^2 and θ_{002}^2 are all similar to that of θ_{002}. The convergence of the autocorrelation functions of the squares of the remaining six modes was better than the convergence of the autocorrelation functions of the modes themselves. Also, all manifestly decay towards zero. This suggests that the regions in which these six modes become vanishingly small may be causing the problems with convergence: their contribution becomes negligible when the square is taken.

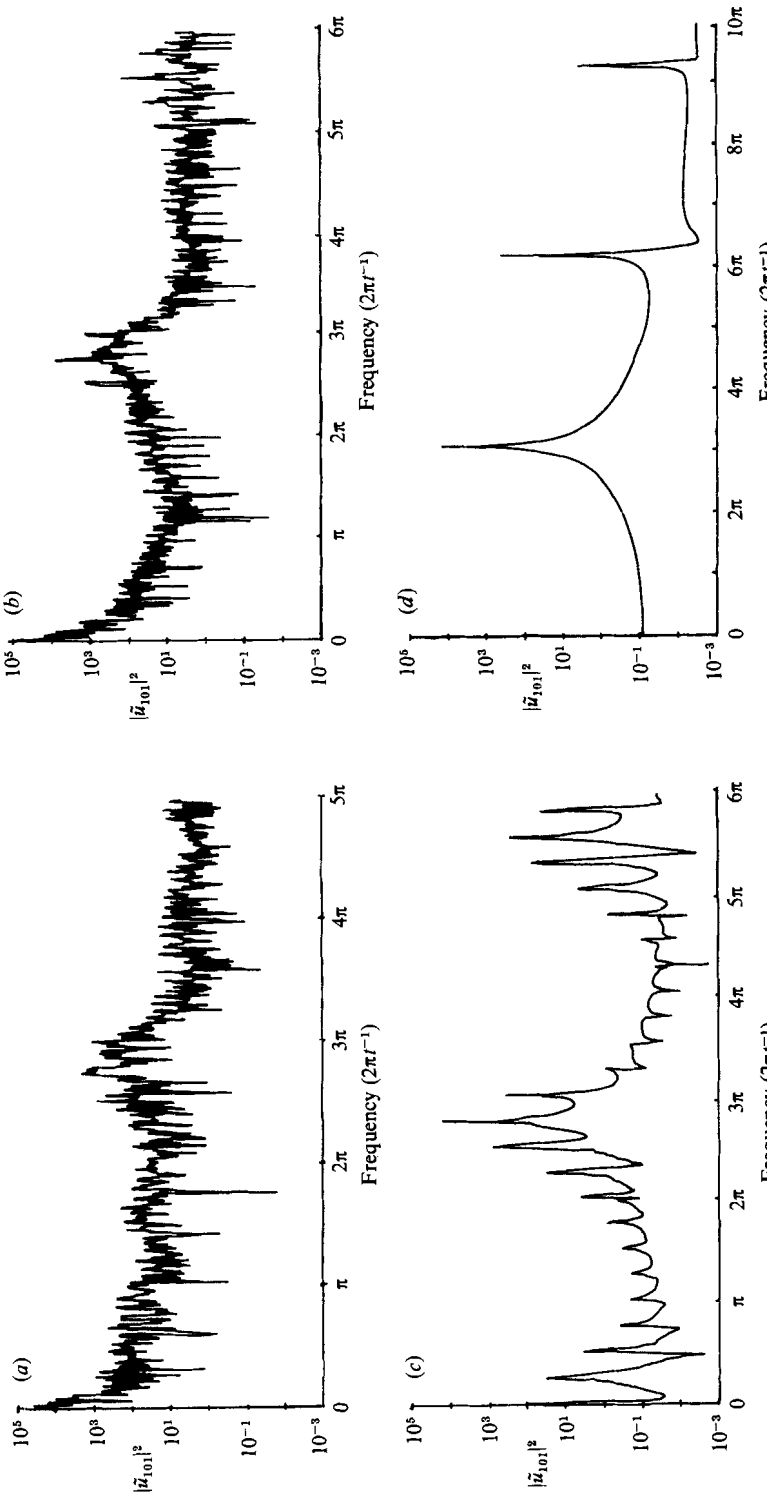

FIGURE 12. Spectra of $u_{101}(t)$ from the nine-mode system for $Pr = 10$, $b = \frac{8}{3}$ and (*a*) $r = 26.0$; (*b*) $r = 26.25$; (*c*) $r = 26.6$; (*d*) $r = 35.0$.

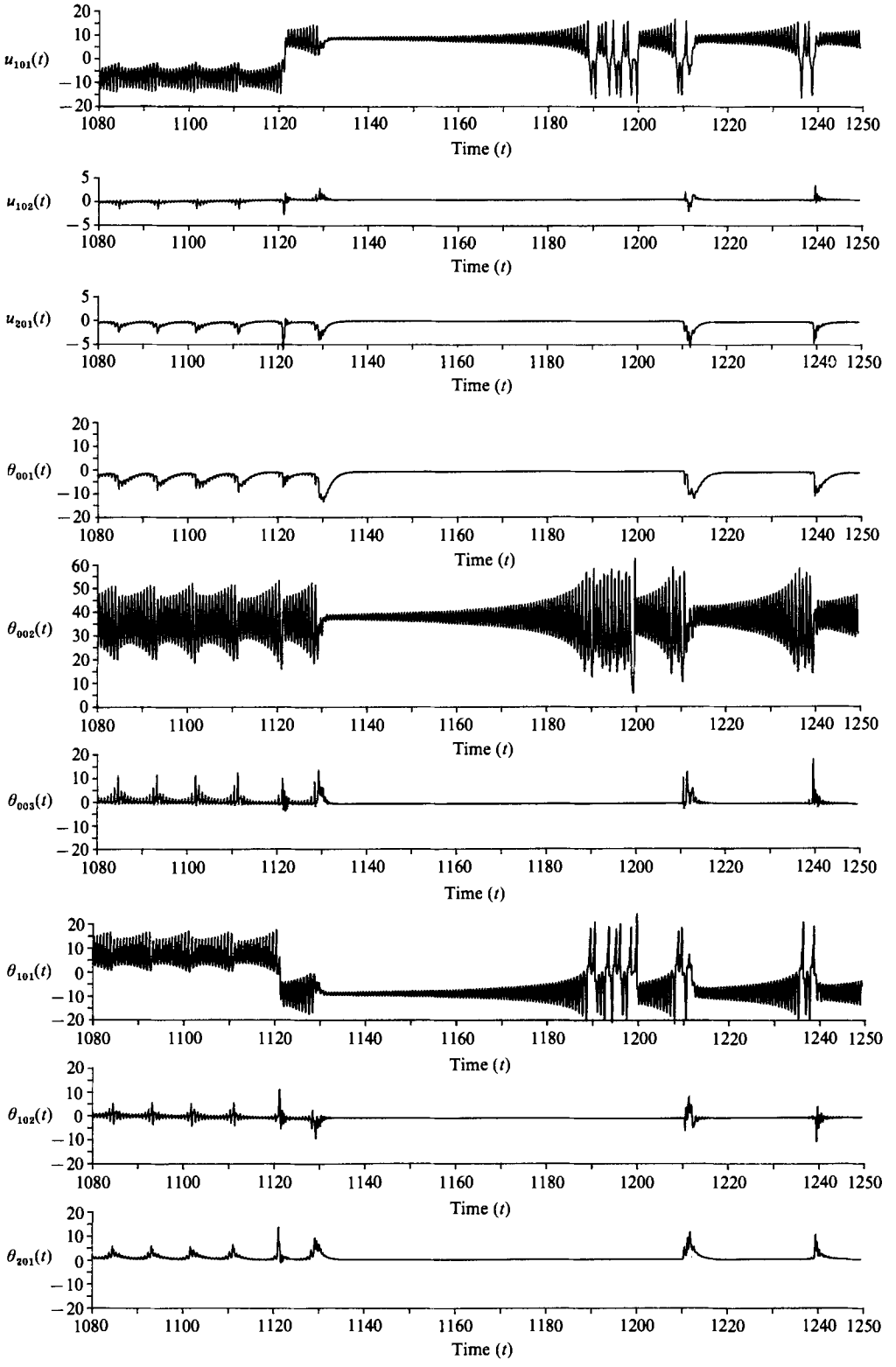

FIGURE 13. Typical time series of the coefficients in the nine-mode system for $r = 26$, $Pr = 10$ and $b = \frac{2}{3}$.

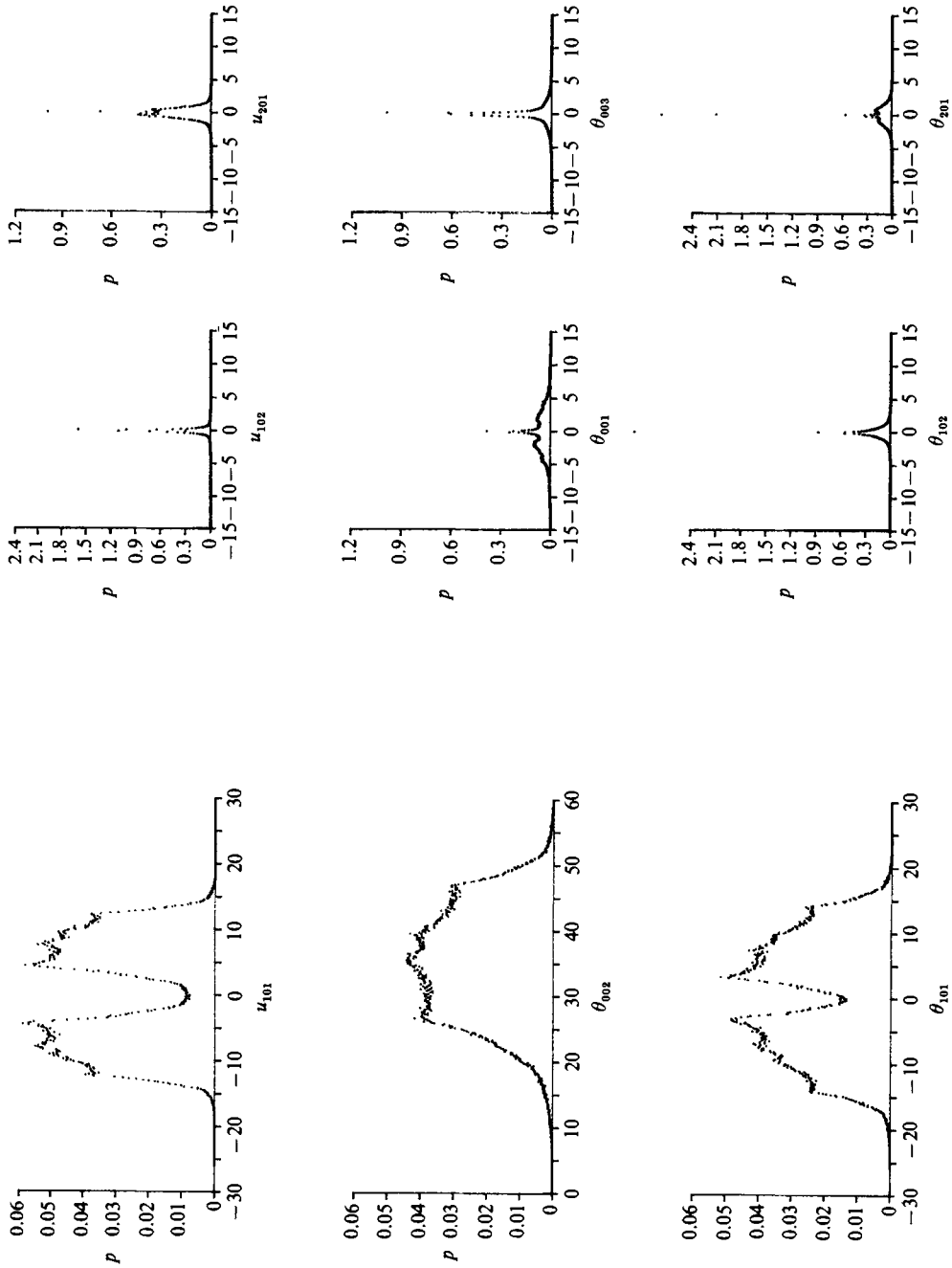

FIGURE 14. Probability density functions of the coefficients for $r = 26$, $Pr = 10$ and $b = \frac{8}{3}$.

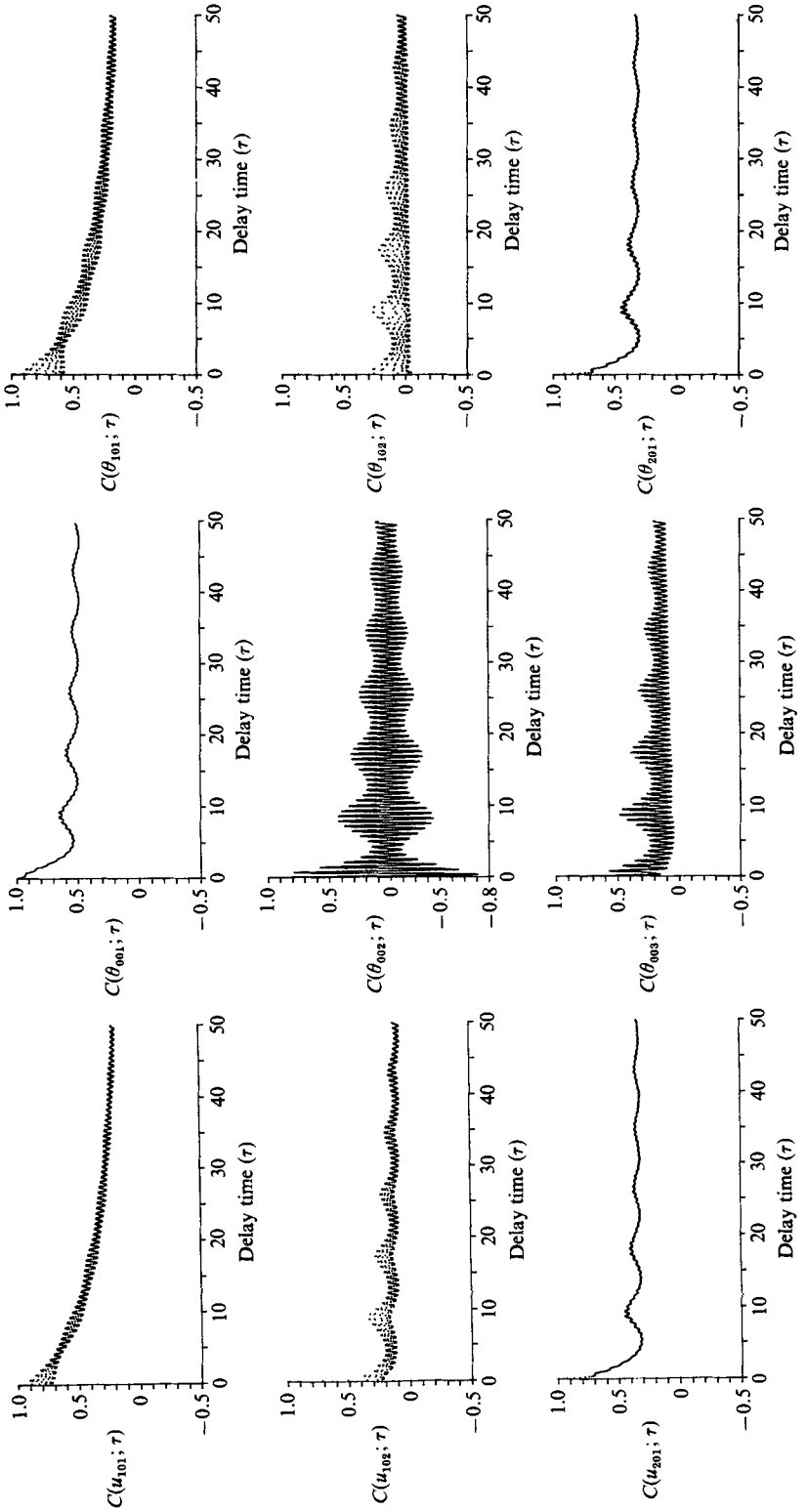

FIGURE 15. Autocorrelation functions of the coefficients for $r = 26$, $Pr = 10$ and $b = \frac{8}{3}$.

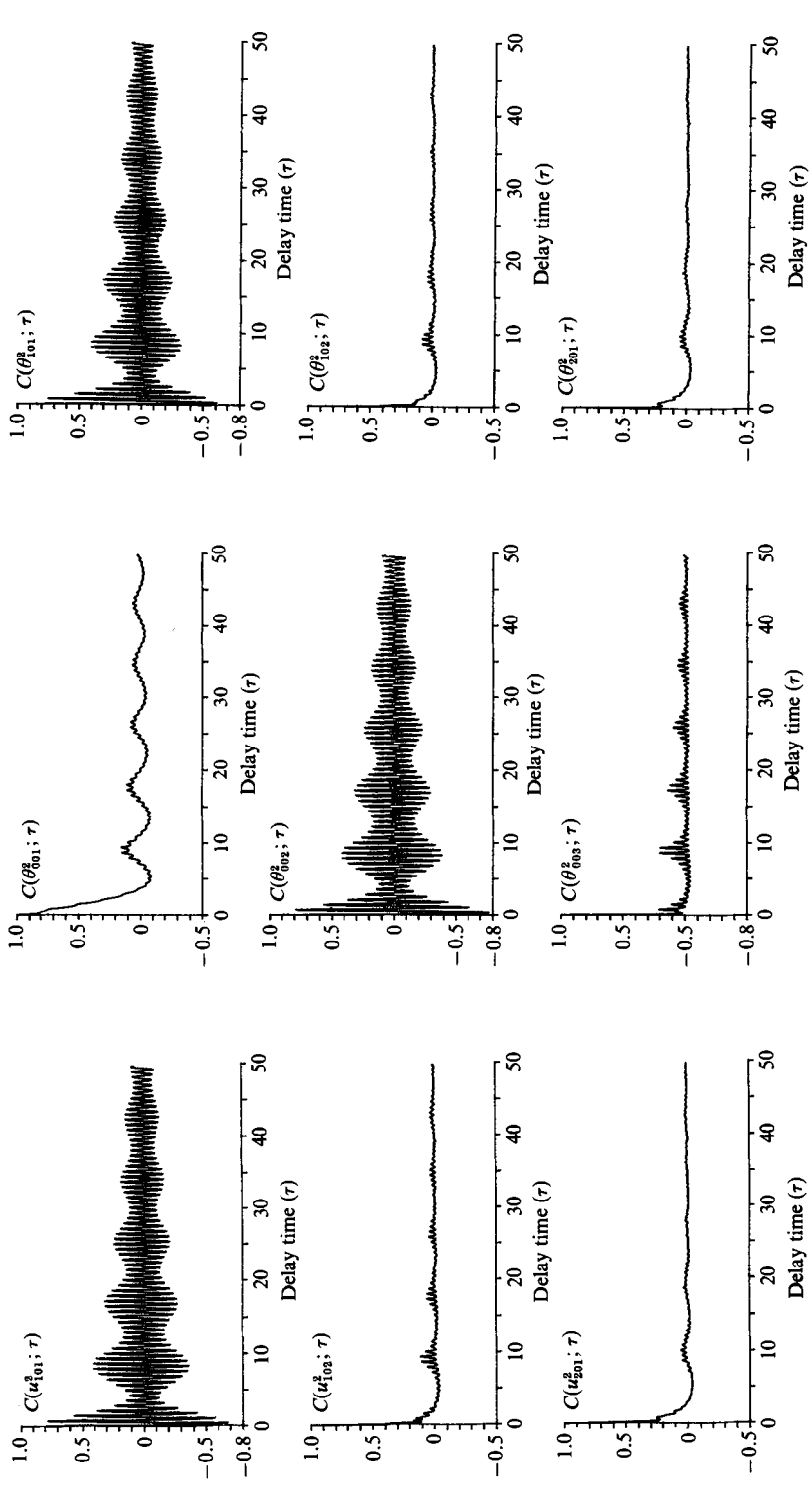

FIGURE 16. Autocorrelation functions of the squares of the coefficients for $r = 26$, $Pr = 10$ and $b = \frac{8}{3}$.

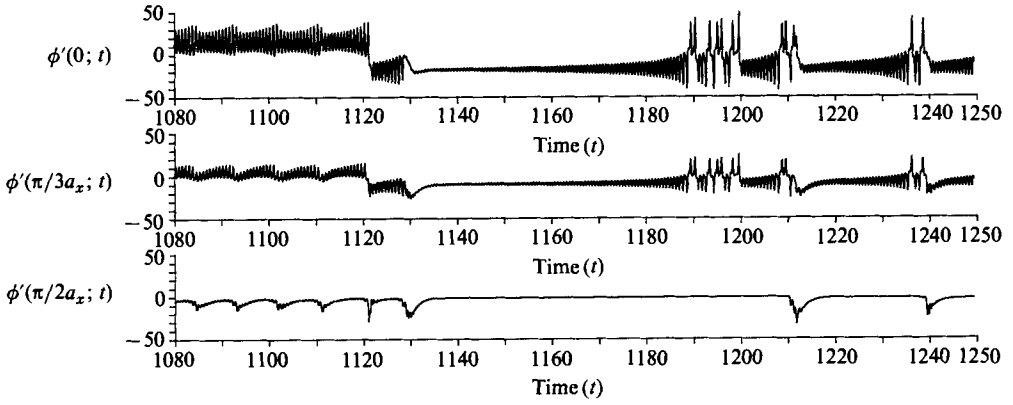

FIGURE 17. Time series of the phase ϕ' at different horizontal positions.

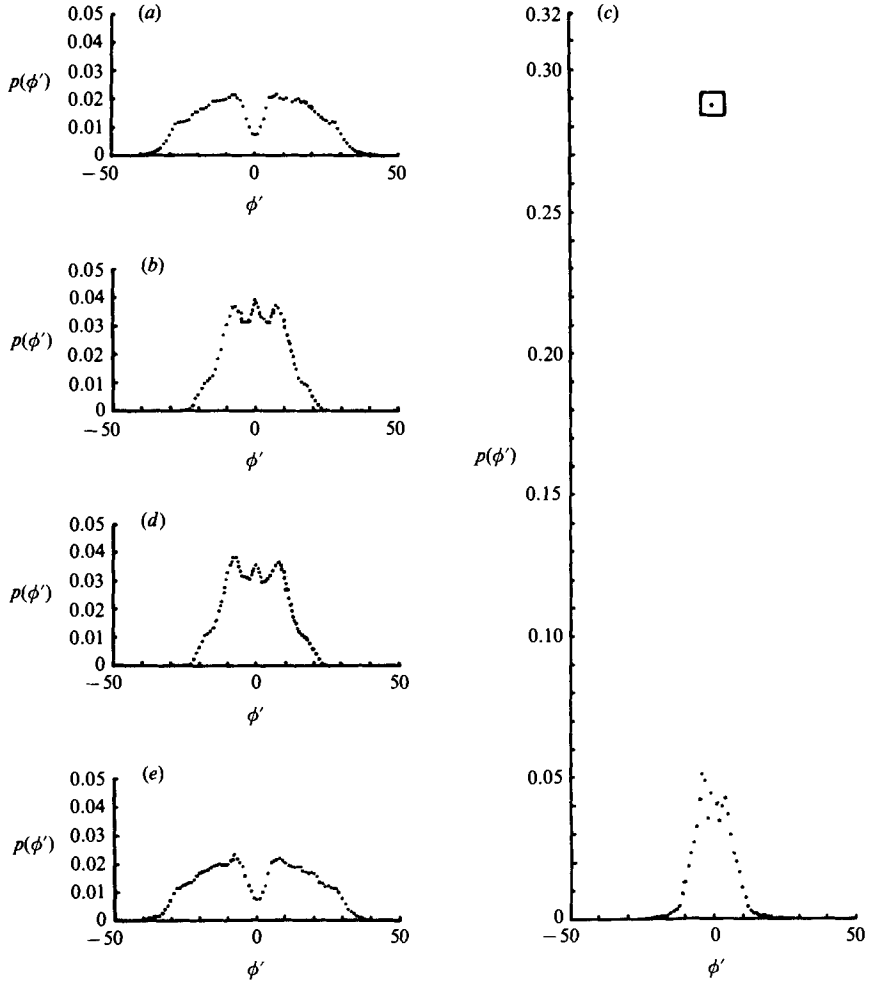

FIGURE 18. Probability density function of ϕ' at (*a*) $a_x x = 0$; (*b*) $a_x x = \frac{1}{3}\pi$; (*c*) $a_x x = \frac{1}{2}\pi$; (*d*) $a_x x = \frac{2}{3}\pi$; (*e*) $a_x x = \pi$.

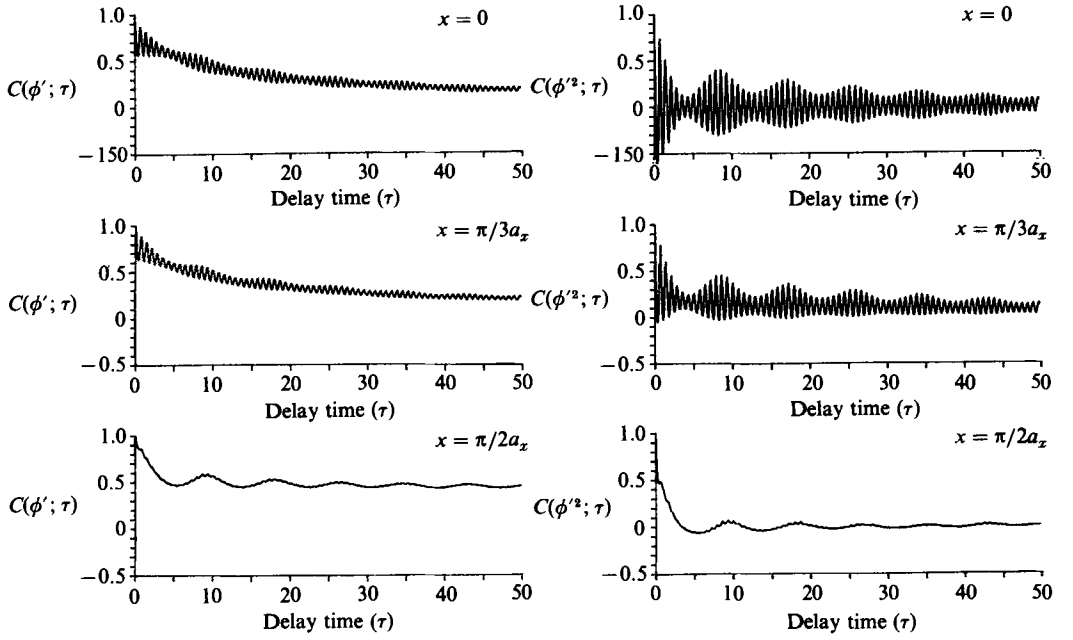

FIGURE 19. Autocorrelation functions of ϕ' and ϕ'^2.

The phase shift produced by a hypothetical fluid obeying this model is

$$\phi(x;t) = k(n_0 - 1 + \tfrac{1}{2}n_0\eta R) - \frac{4kn_0\eta R_c\phi'(x;t)}{3\pi^2}, \tag{5.6}$$

where

$$\phi'(x;t) = \theta_{001}(t) + \tfrac{1}{3}\theta_{003}(t) + 2\theta_{101}(t)\cos(a_x x) + 2\theta_{201}(t)\cos(2a_x x). \tag{5.7}$$

Typical time series of $\phi'(x;t)$, at different values of x, are shown in figure 17. The coefficient $\theta_{101}(t)$ dominates except near the points $a_x x = (n+\frac{1}{2})\pi$, and hence the series are nearly symmetric about these points. It is interesting that such an abrupt change of behaviour is found over the small regions near to these points.

The probability density functions, autocorrelation functions and autocorrelation functions of the square, of the phase are shown in figures 18 and 19. Again, the dominance of the coefficient θ_{101} is apparent. All these properties were found to be symmetric about $a_x x = \frac{1}{2}\pi$. This symmetry is not inconsistent with the sign of θ_{101} being independent of the signs of the other three.

6. Discussion

The two preceding sections have shown some interesting results and highlighted some important problems. The need to truncate carefully is well known; our results have shown how the behaviour of the dominant modes may be significantly altered by the presence of extra modes with only very small amplitude. Much higher-order truncations are needed to give reliable quantitative statistical properties of convection in a real fluid. Three-dimensional effects, and movement of the convection pattern must be represented. However, we might expect some qualitative features to be similar to those observed for these two simple models.

The problems highlighted by this work mainly concern convergence of the

statistical properties. Series of at least several hours duration in real time are likely to be needed, making it difficult to hold the external conditions steady throughout the course of the experiment. Moreover, there is no *a priori* method of estimating more closely the length of series needed to give statistical convergence. To use trial and error is inconvenient, and may be costly. Time series produced numerically may easily be extended, provided the final point is stored in a sufficiently accurate form. Those obtained experimentally may not, and the entire experiment must be repeated if convergence is found to be unsatisfactory. It may be useful to calculate running averages as the data are collected, in order to test the convergence as the experiment progresses.

Another problem is that of distinguishing long-lived chaotic transients, which may occur prior to regular motion, from true chaos. They can occur in both numerical and experimental work: Grebogi, Ott & Yorke (1983) discuss this with respect to theoretical work, and Croquette, Mory & Schosseler (1983) report experimental observations of the phenomenon. In principle, it may be possible to identify transients which gradually decay towards regular motion as such, but those which end abruptly might not be recognized before the final state is reached. This problem is aggravated by the length of series needed. It is impossible to inspect the complete series graphically, and difficult to ensure that any parts which are inspected, though randomly chosen, are typical. Thus careful processing of the data is required to detect any abnormal events. The development of the probability density functions with the length of the series may prove useful for this.

Some preliminary experimental results have been processed, and are discussed briefly by Hawkins (1984). The probability density function of the phase shift shows some evidence of side peaks, similar to those in figures 3, 4 and 14, but the autocorrelation functions of the phase and of its square show disappointingly little structure. However, these data are known to contain significant errors, and more accurate results must be obtained before any conclusions can be drawn. Work to improve the accuracy of the experimental data is in progress, and the results will be reported elsewhere.

In conclusion, we have shown that light-scattering techniques may provide quantitative information about the temperature field of a convecting fluid, and that measurements of the phase are more useful than those of the intensity. We have calculated statistical properties of two simple models operating in the chaotic regime. The numerical work requires significant amounts of computer resources, and the experimental work requires great care. Nevertheless, the work described here appears to provide a useful approach to investigating the connection between strange attractors and turbulence, as well as providing a non-invasive technique of measuring turbulence.

I would like to thank Professor P. G. Drazin and Dr E. Jakeman for their help with this work, and Dr J. H. Hannay for some useful discussions.

The financial support of the Science and Engineering Research Council, and the Royal Signals and Radar Establishment, Great Malvern, is gratefully acknowledged.

REFERENCES

BENETTIN, G., CASARTELLI, M., GALGANI, L., GIORGILLI, A. & STRELCYN, J. M. 1978 On the reliability of numerical studies of stochasticity. I. Existence of time averages. *Nuovo Cim.* **44B**, 183–195.

BERRY, M. V. 1977 Focusing and twinkling: critical exponents from catastrophes in non-Gaussian random short waves. *J. Phys.* A **10** (12), 2061–2081.

BLEISTEIN, N. & HANDELSMAN, R. A. 1975 *Asymptotic Expansion of Integrals*, pp. 340–353. Holt, Rinehart & Winston.

CROQUETTE, V., MORY, M. & SCHOSSELER, F. 1983 Rayleigh–Bénard convective structures in a cylindrical container. *J. Physique* **44**, 293–301.

CURRY, J. H., HERRING, J. R., LONCARIC, J. & ORSZAG, S. A. 1984 Order and disorder in two- and three-dimensional Bénard convection. *J. Fluid Mech.* **147**, 1–38.

DRAZIN, P. G. & REID, W. H. 1982 *Hydrodynamic Stability*. Cambridge University Press.

FOIAS, C. & TEMAM, R. 1983 Asymptotic numerical analysis for the Navier–Stokes equations. In *Nonlinear Dynamics and Turbulence* (ed. G. I. Barenblatt, G. Iooss & D. D. Joseph), ch. 8, pp. 139–155. Pitman.

GREBOGI, C., OTT, E. & YORKE, J. A. 1983 Fractal basin boundaries, long-lived chaotic transients, and unstable–unstable pair bifurcation. *Phys. Rev. Lett.* **50**, 935–938.

GROSSMANN, S. & SONNEBORN-SCHMICK, B. 1982 Correlation decay in the Lorenz model as a statistical physics problem. *Phys. Rev.* A **25**, 2371–2384.

HAWKINS, S. C. 1984 The scattering of light by a chaotically convecting fluid. Ph.D. thesis, University of Bristol.

JONES, D. S. 1964 *The Theory of Electromagnetism*, p. 343. Pergamon.

KNOBLOCH, E. 1978 On the statistical dynamics of the Lorenz model. *J. Stat. Phys.* **20**, 695–708.

LANFORD, O. E. 1981 Strange attractors and turbulence. In *Hydrodynamic Instabilities and the Transition to Turbulence* (ed. H. L. Swinney & J. P. Gollub), Topics in applied physics, vol. 45. Springer.

LORENZ, E. N. 1963 Deterministic nonperiodic flow. *J. Atmos. Sci.* **20**, 130–141.

LÜCKE, M. 1976 Statistical dynamics of the Lorenz model. *J. Stat. Phys.* **15**, 455–475.

MCLAUGHLIN, J. B. & MARTIN, P. C. 1975 Transition to turbulence in a statically stressed fluid system. *Phys. Rev.* A **12**, 186–203.

RUELLE, D. & TAKENS, F. 1971 On the nature of turbulence. *Comm. Math. Phys.* **20**, 167–192.

SMITH, H. 1977 The validity of statistical results from N-body calculations. *Astron. Astrophys.* **61**, 305–312.

SPARROW, C. 1982 *The Lorenz Equations: Bifurcations, Chaos, and Strange Attractors*. Springer.